

This is a **preprint** of the published article:

Riedesel, S., Jain, M., 2024. Excited state lifetime of electron trapping centres in alkali feldspars. *Radiation Measurements* 172, 107081. <https://doi.org/10.1016/j.radmeas.2024.107081>

This is a **preprint** of the published article:

Riedesel, S., Jain, M., 2024. Excited state lifetime of electron trapping centres in alkali feldspars. *Radiation Measurements* 172, 107081. <https://doi.org/10.1016/j.radmeas.2024.107081>

## Excited state lifetime of electron trapping centres in alkali feldspars

Svenja Riedesel<sup>a,b</sup> and Mayank Jain<sup>a</sup>

<sup>a</sup> Radiation Physics Division, Department of Physics, Technical University of Denmark, Risø Campus, Roskilde, Denmark

<sup>b</sup> Institute of Geography, University of Cologne, Cologne, Germany

### Abstract

The development of the infrared photoluminescence (IRPL) signal enables the direct non-destructive probing of the trapped electron population in feldspars. Whilst IRPL offers new perspectives for luminescence dating, it also enables detailed, site-selective measurements of the dosimetric defects emitting IRPL at 880 nm (IRPL<sub>880</sub>) and 955 nm (IRPL<sub>955</sub>), allowing improved understanding of luminescence phenomena in feldspars.

We perform time-resolved IRPL measurements to investigate the excited state lifetimes of IRPL<sub>880</sub> and IRPL<sub>955</sub> electron trapping centres in chemically and structurally different feldspars. We analyse the time-resolved off-time data with three exponentially decaying components. The contribution of the fast component ( $\tau_1$ ) fitted to the IRPL<sub>880</sub> data is minor and its lifetime is consistent with the switch off time of the 830 nm excitation laser. The two longer lifetimes ( $\tau_2$  and  $\tau_3$ ) dominate the IRPL<sub>880</sub> and IRPL<sub>955</sub> signals. The  $\tau_2$  values range from 2  $\mu$ s to 6  $\mu$ s for IRPL<sub>880</sub> and from 2  $\mu$ s to 7  $\mu$ s for IRPL<sub>955</sub>, whereas  $\tau_3$  ranges from 7  $\mu$ s to 25  $\mu$ s for IRPL<sub>880</sub> and from 8  $\mu$ s to 22  $\mu$ s for IRPL<sub>955</sub>, with an average cluster value of  $\sim 20$   $\mu$ s. We observe a weak decreasing trend in  $\tau_3$  lifetime with decreasing K-feldspar content. Systematic thermal depletion of the trapped electron population results in decreasing  $\tau_2$  lifetimes with increasing preheat temperature, but a negligible change in  $\tau_3$ . We suggest that time-resolved-IRPL lifetimes not only reflect the excited state lifetime of the electron trapping centre, affected by excited-to-ground state transition as well as tunnelling, but also a direct recombination from the band tail states. The long excited-state lifetime of the order of 20  $\sim$   $\mu$ s (the average cluster value) allows for tunnelling induced recombination from the excited state, which is supported by the fact that reported lifetimes for time-resolved-IRSL (infra-red stimulated luminescence) are shorter than those of time-resolved-IRPL.

## Excited state lifetime of electron trapping centres in alkali feldspars

Svenja Riedesel<sup>a,b</sup> and Mayank Jain<sup>a</sup>

<sup>a</sup> Radiation Physics Division, Department of Physics, Technical University of Denmark, Risø Campus, Roskilde, Denmark

<sup>b</sup> Institute of Geography, University of Cologne, Cologne, Germany

### Abstract

The development of the infrared photoluminescence (IRPL) signal enables the direct non-destructive probing of the trapped electron population in feldspars. Whilst IRPL offers new perspectives for luminescence dating, it also enables detailed, site-selective measurements of the dosimetric defects emitting IRPL at 880 nm (IRPL<sub>880</sub>) and 955 nm (IRPL<sub>955</sub>), allowing improved understanding of luminescence phenomena in feldspars.

We perform time-resolved IRPL measurements to investigate the excited state lifetimes of IRPL<sub>880</sub> and IRPL<sub>955</sub> electron trapping centres in chemically and structurally different feldspars. We analyse the time-resolved off-time data with three exponentially decaying components. The contribution of the fast component ( $\tau_1$ ) fitted to the IRPL<sub>880</sub> data is minor and its lifetime is consistent with the switch off time of the 830 nm excitation laser. The two longer lifetimes ( $\tau_2$  and  $\tau_3$ ) dominate the IRPL<sub>880</sub> and IRPL<sub>955</sub> signals. The  $\tau_2$  values range from 2  $\mu$ s to 6  $\mu$ s for IRPL<sub>880</sub> and from 2  $\mu$ s to 7  $\mu$ s for IRPL<sub>955</sub>, whereas  $\tau_3$  ranges from 7  $\mu$ s to 25  $\mu$ s for IRPL<sub>880</sub> and from 8  $\mu$ s to 22  $\mu$ s for IRPL<sub>955</sub>, with an average cluster value of  $\sim$ 20  $\mu$ s. We observe a weak decreasing trend in  $\tau_3$  lifetime with decreasing K-feldspar content. Systematic thermal depletion of the trapped electron population results in decreasing  $\tau_2$  lifetimes with increasing preheat temperature, but a negligible change in  $\tau_3$ . We suggest that time-resolved-IRPL lifetimes not only reflect the excited state lifetime of the electron trapping centre, affected by excited-to-ground state transition as well as tunnelling, but also a direct recombination from the band tail states. The long excited-state lifetime of the order of 20  $\sim$   $\mu$ s (the average cluster value) allows for tunnelling induced recombination from the excited state, which is supported by the fact that reported lifetimes for time-resolved-IRSL (infra-red stimulated luminescence) are shorter than those of time-resolved-IRPL.

### Keywords

Feldspars, photoluminescence, time-resolved luminescence, IRPL, lifetime

### 1 Introduction

Feldspars are wide band gap materials with the ability to trap and store charge within defects in their crystal lattice, enabling their use as natural dosimeters to constrain depositional histories in

This is a **preprint** of the published article:

Riedesel, S., Jain, M., 2024. Excited state lifetime of electron trapping centres in alkali feldspars. *Radiation Measurements* 172, 107081. <https://doi.org/10.1016/j.radmeas.2024.107081>

archaeological and geological contexts. The charge storage ability of feldspars is affected by an athermal signal loss, termed fading (Wintle, 1973; Visocekas, 1985), which, unless corrected for, leads to age underestimation (Huntley and Lamothe, 2001; Kars et al., 2008). However, over the past one and a half decades advances in feldspar luminescence have helped to minimise the impact of fading on the luminescence results (cf. Thomsen et al., 2008; Thiel et al., 2011; Li and Li, 2011; Prasad et al., 2017). One of these advances is the development of infrared photoluminescence (IRPL; Prasad et al., 2017). IRPL not only lowers fading compared to conventional, recombination-based luminescence techniques (Kumar et al., 2020), such as infrared stimulated luminescence (IRSL; Hütt et al., 1988), it also enables the non-destructive probing of trapped electrons within electron trapping centres in the feldspar lattice (Prasad et al., 2017).

Excitation spectra of feldspars reveal a strong resonance peak in the infrared ( $\sim 1.45$  eV; Hütt et al., 1988, Kars et al., 2013, Riedesel et al., 2018). Stimulating irradiated feldspars with IR photons, causes excitation of electrons from the ground state of the electron trapping centres to the excited state. Radiative excited- to ground-state transition within the electron trapping centres results in the emission of IR photons with energies of 1.3 eV ( $\sim 955$  nm) and 1.41 eV ( $\sim 880$  nm). These two main IRPL emissions, henceforth termed IRPL<sub>880</sub> and IRPL<sub>955</sub>, have been detected in feldspars and have been associated with two different defect sites in the crystal (Kumar et al. 2018; Jain et al., 2020; Riedesel et al., 2021a). However, the crystal defects functioning as electron trapping centres in feldspars are yet to be identified. Time-resolved luminescence techniques allow the measurement of excited- to ground-state relaxation times within a defect and thus help to improve our understanding the type of defect and transition (i.e. allowed or spin-forbidden) involved in the luminescence process.

Conventional luminescence measurements utilise continuous wave (CW) stimulation. In these CW luminescence measurements, sample material is stimulated using LEDs or laser diodes for a given amount of time, usually tens to hundreds of seconds. During these CW stimulations, the sample's (anti-Stokes) emission is recorded by a photomultiplier (PMT), or by a (electron multiplying) charge coupled device ((EM)-CCD). In contrast, during time-resolved measurements the excitation light source is pulsed on and off and the emission is recorded during on- and off-times. In many cases, also in the present study, the emitted photons are detected using time-correlated single-photon counting (TCSPC; Lapp et al., 2009). TCSPC allows recording the arrival time of each photon at the detector. Summing the luminescence response of several thousand pulses results in the photon arrival time distribution, which can then be used for fitting the off-time decay to obtain lifetimes of the excited state of the defect probed during the measurement.

Time-resolved luminescence measurements of feldspars have been performed previously. Most of these focussed on characterising feldspar IRSL emissions in the UV, blue, yellow-green and red, in order

This is a **preprint** of the published article:

Riedesel, S., Jain, M., 2024. Excited state lifetime of electron trapping centres in alkali feldspars. *Radiation Measurements* 172, 107081. <https://doi.org/10.1016/j.radmeas.2024.107081>

to understand the defects and transitions involved in electron-hole recombination processes in feldspars (e.g. Sanderson and Clark, 1994; Clark et al., 1997; Clark and Bailiff, 1998; Tsukamoto et al., 2006; Ankjærgaard and Jain, 2010; Jain and Ankjærgaard, 2011; Pagonis et al., 2012; Riedesel et al., 2023). Whilst considerable effort has been put into understanding the luminescence centres probed by electron-hole recombination in feldspars and their resulting luminescence, only very little is known about the excited state lifetime within the electron trapping centres in feldspars. Prasad et al. (2017) investigated three different feldspar samples and measured the off-time IRPL<sub>955</sub> emission at room temperature (295 K) and at 7 K. They found that it was possible to describe the data by fitting a single exponential function to the data and obtained average lifetimes of ~30 µs and ~40 µs for their 295 K and 7 K measurements, respectively. These lifetimes are interpreted to reflect the excited state lifetime of the IRPL<sub>955</sub> defect at the two different temperatures measured. Kumar et al. (2020) performed TCSPC-based lifetime measurements on one feldspar sediment extract (R47), which was also investigated by Prasad et al. (2017). Kumar et al. (2020) obtained lifetimes of 20 µs for the off-time for both IRPL<sub>880</sub> and IRPL<sub>955</sub> signals at room temperature, which is faster than the lifetime obtained by Prasad et al. (2017) for the same sample. Besides the two studies by Prasad et al. (2017) and Kumar et al. (2020) no detailed investigations have been made into the lifetimes of the IRPL<sub>880</sub> and IRPL<sub>955</sub> emissions.

Here we aim at investigating the dependence of IRPL lifetime, which is a fundamental characteristic of the electron trapping centre, describing its excited- to ground-state transition, on composition and structure of selected alkali feldspars. To further constrain our understanding of the processes influencing the lifetime, we also investigate the effect of detrapping through preheating at different temperatures on the IRPL<sub>880</sub> and IRPL<sub>955</sub> lifetimes.

## **2 Material and methods**

### **2.1 Sample material**

A suite of eleven chemically and structurally different single crystal alkali feldspar samples, including K- and Na-feldspar end members, was used in this study. The samples investigated here reflect the range of alkali feldspars found in nature. Ordered single phase feldspars, with microcline as the K-feldspar end member and albite as the Na-feldspar end member, are rather rare occurrences. In these crystals Si<sup>4+</sup> and Al<sup>3+</sup> tetrahedra form the framework, whilst K<sup>+</sup> and Na<sup>+</sup> ions are located in the cavities of the framework. Whilst end members contain one type of these cations (either Na<sup>+</sup> or K<sup>+</sup>), perthites contain both. The difference in ionic radii of K<sup>+</sup> and Na<sup>+</sup> ions drive the formation of exsolution lamellae in perthitic feldspars during cooling of rocks. Whilst all of these described feldspars form during slower cooling, for instance in plutonic igneous or metamorphic rocks, disordered feldspars form by rapid

This is a **preprint** of the published article:

Riedesel, S., Jain, M., 2024. Excited state lifetime of electron trapping centres in alkali feldspars. *Radiation Measurements* 172, 107081. <https://doi.org/10.1016/j.radmeas.2024.107081>

cooling in e.g. volcanic rocks, during which the high temperature structural state (disorder of Si<sup>4+</sup> and Al<sup>3+</sup> ions on the framework) of the feldspar is retained (Deer et al., 2013).

Details regarding the samples' origin, their chemical composition, and on the mineral phases present in the specimens are given in Table 1. The chemical composition (relative contribution of the main feldspar phases, %) was determined from quantitative X-ray fluorescence (XRF) data using stoichiometry. Semi-quantitative phase analysis results are based on X-ray diffraction (XRD) data. Details on the instrumentation used for XRF and XRD measurements are explained in Riedesel et al. (2021b). Samples FSM-13LH and FSM-6LH are artificially disordered counterparts of samples FSM-13 and FSM-6. FSM-13LH and FSM-6LH were heated to 1050 °C in a furnace for 5 days (FSM-6LH) and 10 days (FSM-13LH) to disorder the (Si,Al)-framework. To retain the disordered structure the samples were rapidly cooled to room temperature. The disordered structure was validated using XRD. Further details regarding this experiment and the obtained X-ray diffraction patterns can be found in Riedesel (2020) and Riedesel et al. (2021b). The luminescence behaviour of the samples has been studied previously and results from excitation and emission spectroscopy of the samples can be found in Riedesel et al. (2019, 2021a and 2021b). Time-resolved IRSL measurements were also performed on some of the samples and the results are presented in Riedesel et al. (2023).

## 2.1 Instrumentation

All time-resolved measurements were made on a Risø TL/OSL DA20 reader located at the Radiation Physics Division, Department of Physics, Technical University of Denmark. The luminescence reader is equipped with a <sup>90</sup>Sr/<sup>90</sup>Y source delivering ~0.1 Gy s<sup>-1</sup> at sample position. The luminescence is excited by using an IR (830 nm) 140 mW TTL modulated laser passing through a diffuser to obtain a uniform power distribution on the sample disc. The emitted luminescence is detected by a Hamamatsu H7421-50 (380-890 nm) PMT through a combination of two LP850 and LP880/10 nm BP filters for the IRPL<sub>880</sub> emission and by a Hamamatsu H10330C-25 (950-1200 nm) PMT through a combination of two LP925 and 950/50AP BP filters to isolate the IRPL<sub>955</sub> emission.

Table 1. Details regarding the chemical composition and mineral phases present for samples investigated. The chemical composition in % feldspars, was calculated from semi-quantitative XRF data using stoichiometric conversion. Mineral phases present were estimated based on semi-quantitative XRD analyses.

Sample ID	Origin	Chemical composition (FS %)			Microcline	Phases present		
		K-FS	Na-FS	Ca-FS		Orthoclase	Sanidine	Albite
FSM-13	Brazil	98.5	1.5	0.0	100	-	-	-
FSM-13LH	Brazil	98.5	1.5	0.0	100	-	-	-
FSM-3	Granite pegmatite, Toe Head, South Harris, Scotland, UK (Cunningham, 1981)	82.5	17.2	0.3	78	-	-	22
FSM-15	Buckingham, Quebec, Canada	80.4	19.6	0.0	82	-	-	18
FSM-7	Unknown	76.8	22.0	1.2	48	-	-	51
FSM-5	Unknown	74.8	25.20	0.0	57	-	-	43
FSM-6	Granite pegmatite, Trezaise Quarry, Cornwall, UK (Ussher et al., 1909)	74.4	25.3	0.3	-	38	-	62
FSM-6LH	Trezaise Quarry, Cornwall, UK	74.4	25.3	0.3	-	-	100	-
FSM-11	Perth, Canada	65.2	34.8	0.0	62	-	-	38
Al-I	Pinzele, Trente, Italy (Govindaraju, 1995)	1.0	97.0	2.0	-	-	-	-
CLBR	Pegmatite, Golonca District, Minas Gerais, Brazil (Cassadanne and Roditi, 1996)	0.5	99.3	0.2	-	-	-	100

## 2.2 Experimental setup

Two different measurement protocols were used to gain insights into the lifetimes and the stability of the IRPL<sub>880</sub> and IRPL<sub>955</sub> signals and the two protocols are outlined in Tables 2 and Table 3. The same aliquots were used for all measurements and two aliquots were measured per sample. The aliquots were made by placing the sample (either as shards or powder) on the stainless-steel cups. No adhesive agent was used.

To minimise the potential influence of sensitivity change on the measurement results, all aliquots were stimulated with two consecutive IRSL measurements at 290°C (IRSL<sub>290</sub>) for 100s prior to the first pulsed IRPL measurement. The second of these consecutive IRSL<sub>290</sub> measurements served as a measure for any potential remaining background signal, which was found to be negligible for all samples. Following the IRSL<sub>290</sub> bleach the samples were given a 5 Gy beta dose before performing the remaining TL, IRSL and/or IRPL measurements.

The first measurement protocol (Table 2) was used to measure the lifetimes of the IRPL<sub>880</sub> and IRPL<sub>955</sub> signals following a preheat at 250 °C for 60 s using three different on-time durations (pulse width) for

the 830 nm laser stimulation (5, 10 and 20  $\mu$ s). The protocol outlined in Tables 3 test for the lifetime dependence of the IRPL<sub>880</sub> and IRPL<sub>955</sub> signals on prior heating (after dose).

Table 2. Measurement protocol for time-resolved IRPL signals after a preheat at 250 °C, with different on-time durations. On-time duration of 5, 10 and 20  $\mu$ s were tested for time-resolved IRPL signals.

Step	Treatment
1	CW-IRSL at 290 °C for 100 s (bleach)
2	CW-IRSL at 290 °C for 100 s (bleach)
3	5 Gy beta dose
4	TL at 250 °C for 60 s, 2 °C/s
5	Time-resolved IRPL <sub>880</sub> for 10 s at 30 °C
6	Time-resolved IRPL <sub>955</sub> for 10 s at 30 °C

Table 3. Measurement protocol for pulse anneal experiments.

Step	Treatment
1	CW-IRSL at 290 °C for 100 s (bleach)
2	CW- IRSL at 290 °C for 100 s (bleach)
3	IRPL <sub>880</sub> for 10 s at 30 °C, On-time: 20 $\mu$ s, Off-time: 80 $\mu$ s
4	IRPL <sub>955</sub> for 10 s at 30 °C, On-time: 20 $\mu$ s, Off-time: 80 $\mu$ s
5	5 Gy beta dose
6	TL to 50 at 2°C/s
7	IRPL <sub>880</sub> for 10 s at 30 °C, On-time: 20 $\mu$ s, Off-time: 80 $\mu$ s
8	IRPL <sub>955</sub> for 10 s at 30 °C, On-time: 20 $\mu$ s, Off-time: 80 $\mu$ s
	<i>Return to step 6 and increment TL temperature by 50 °C (until 600 °C).</i>

## 2.3 Fitting

Fitting of time-resolved luminescence signals was done in R using a non-linear least square fitting approach, facilitating the nls() function (Bates and DeRoy, 2018) and using equation 1 for the off-time signal. Here,  $I$  is the intensity at time  $t$ ,  $a_i$  the intensity at time  $t_1$ , where  $t_1$  is the on-time duration, and  $k$  is a constant, representing a stable linear background (e.g. Demas, 1983, p. 39; Chithambo, 2003; Tsukamoto et al., 2006). The data were normalised to the intensity of the last data point of the on-time.

$$I(t) = \sum a_i \exp \left[ - \left( \frac{t-t_1}{\tau_1} \right) \right] + k \quad [1]$$

To obtain information on the contribution of each lifetime to the total off-time signal, we integrated the area under each exponential function and normalised the obtained integral to the sum of the three integrals for each sample to obtain the relative contribution for each component.

## 3 Influence of experimental setup on time-resolved IRPL

Prior to investigating sample-dependent variations of the time-resolved IRPL signals and their response to increasing preheat temperatures, we conducted experiments monitoring the effects of the instrument setup and the experimental conditions. We specifically evaluate different ways of removing the laser breakthrough from the actual IRPL signal (section 3.1) and discuss variations in IRPL<sub>880</sub> and IRPL<sub>955</sub> lifetimes with on-time duration (section 3.2).

### 3.1 Removal of stimulation light breakthrough in the IRPL<sub>880</sub> signal

In our measurement system, the laser switch-off is not instantaneous. Instead, there is an afterglow lasting a few microseconds. Due to the proximity of the excitation light source (830 nm laser) and the detection window of the IRPL<sub>880</sub> emission (880 nm  $\pm$  5 nm at FWHM) an emission from the stimulation light source is also detected. This signal contaminates the recorded IRPL<sub>880</sub> emission (cf. Fig. 1A,B), and the influence can be significant in samples with low IRPL<sub>880</sub> intensity. In the case of IRPL measurements performed in geochronological studies, the pulsing of the laser is enabled, and the off-time signal used for age calculation is recorded as gated signal after discarding the initial 1  $\mu$ s (Kumar et al., 2021) or the initial 3  $\mu$ s (Kook et al., 2017) of the off-time. However, in case of the present study, we are interested in the full off-time signal to make an accurate estimate for any fast-decaying IRPL components. Therefore, it becomes pertinent to characterise the decrease in the intensity of the stimulation laser light pulse in the off-time. This breakthrough also places a limit on the minimum detectable IRPL lifetime in our system.

Table 4. IRPL<sub>880</sub> lifetimes obtained for the laser on different substrates.  $I$  represents the intensity of each component,  $\tau$  the lifetime and  $A$  the amplitude (integrated area under the fitted curve). The different components are denoted using an index number. Prior to fitting the signals were normalised to the last data point of the on-time.

Substrate	$I_1$	$\tau_1$	$A_1$	$I_2$	$\tau_2$	$A_2$	$I_3$	$\tau_3$	$A_3$
Empty cup	1.0	0.1	0.1	0.1	1.6	0.14	0.01	10	0.1
Shard	1.0	0.1	0.1	0.1	1.7	0.14	0.02	15	0.3
Powder	1.0	0.1	0.1	0.1	1.7	0.14	0.01	15	0.15

To constrain the lifetime of the laser off-time we measured the response of the laser on an empty cup and on cups filled with non-IRPL<sub>880</sub> emitting sample material in the form of powder (Al-I) or shards (CLBR, see Riedesel et al., 2021a for emission spectra, which reveal that this feldspar does not exhibit an IRPL<sub>880</sub> emission). The signal was recorded according to the procedure outlined in Table 2, using an on-time duration of 20  $\mu$ s and an off-time duration of 80  $\mu$ s. Figure 1C shows the 830 nm laser breakthrough emission recorded on different substrates, with slightly higher on-time intensities

recorded for the powdered material, likely due to surface-dependent scattering of the incoming laser light. When fitted using equation 1 three lifetime components can be obtained for all three cups and materials tested. The fastest lifetime component (hereafter referred to as lifetime 1,  $\tau_1$ ) dominates the signal with 91 % of the initial signal intensity.  $\tau_1$  decays with a lifetime of 0.1  $\mu\text{s}$ . The two slower lifetime components make up the remaining 9 % of initial signal with  $\tau_2$  decaying with a time 1.6  $\mu\text{s}$  and  $\tau_3$  at 12.7  $\mu\text{s}$  (cf. Fig. 1D, Table 4).

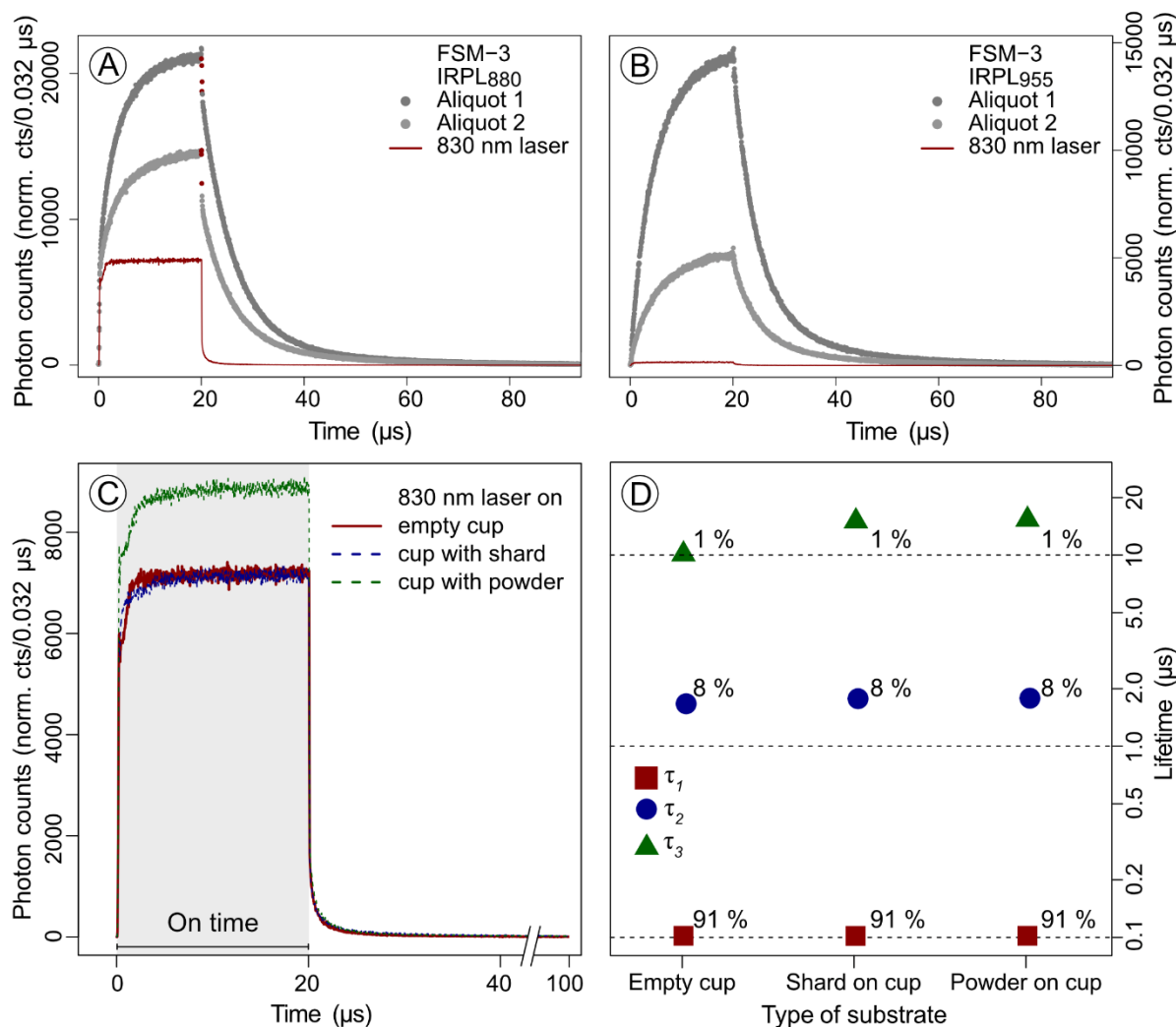


Fig. 1. Comparison of IRPL<sub>880</sub> (A) and IRPL<sub>955</sub> (B) emissions of sample FSM-3 with that of the laser breakthrough recorded for an empty cup. The red dots in the IRPL<sub>880</sub> emission of sample FSM-3 represent the part of the sample signal influenced by the laser breakthrough C) Recorded breakthrough of 830 nm stimulation laser on different substrates for IRPL<sub>880</sub>. The IR laser breakthrough was measured on an empty cup (red line) and on different types of non-IRPL emitting sample material on cups. The latter include a single shard (sample CLBR) and powder (samples AI-I). C) Apparent lifetimes of the laser breakthrough signal in the off-time obtained by fitting a sum of three exponential functions for the different substrates.

When comparing the time-resolved IRPL<sub>880</sub> signal from a sample, in this case FSM-3 (cf. Fig. 1A), to the laser breakthrough, one can see that especially the fastest laser lifetime ( $\tau_1$ ) influences the initial off-time decay of the feldspar sample. To highlight this, the data points reflecting the laser breakthrough are highlighted in red in Fig. 1A. Thus, it is important to deal with this contaminating laser signal to be able to estimate the off-time IRPL decay lifetime(s). We tested three different approaches and compared the results for IRPL<sub>880</sub> signal from five different feldspar samples: FSM-3, FSM-7, FSM-11, FSM-13LH and FSM-15 (Fig. 2). These samples were chosen because of their varying IRPL<sub>880</sub> intensities, thus, enabling us to test the effect of different breakthrough removal approaches on differently luminescent samples.

Firstly, we fitted the IRPL<sub>880</sub> off-time signal of those five samples using equation 1 with three components because this resulted in the best fit to the data. Fitting with two components resulted in large residuals between the measured and fitted data, whereas fitting with four components did not yield a solution. Although three components were also used to describe the signal of the laser, ~90 % of the laser signal is represented by a single lifetime (0.1  $\mu$ s). Therefore, we believe that in the three component fitting of the IRPL<sub>880</sub> signal, the laser contribution can be realistically estimated by a single component ( $\tau_1$ ). The results are used as reference for all three laser removal approaches as described below:

**Approach 1:** As a first approach to remove the laser breakthrough we subtracted the actual laser signal (not the fitted signals) recorded on an empty cup from the sample specific IRPL<sub>880</sub> signal and fitted the thus obtained signal using the sum of three exponential functions. As shown in Figure 1C, the laser signal intensity depends on the light scattering from the sample. Subtracting the laser signal from the sample signal results in negative on-time signal intensities for all samples, which is reflected in a negative intensity ( $I$ ) of  $\tau_1$  in the case of all samples. The intensity is not displayed in Fig. 2, but the column where this is the case is highlighted in Fig. 2.

**Approach 2:** As a second removal approach, we systematically excluded initial data from the off-time signal prior to fitting. The time-resolved data is integrated over bins with a width of 0.032  $\mu$ s. Selecting channels to be excluded from the signal are thus dependent on this binning structure. We considered data removal corresponding to five different time intervals ranging from 0.256  $\mu$ s up to 3  $\mu$ s. We removed the first eight, sixteen and 25 channels of the off time (0.256  $\mu$ s, 0.512  $\mu$ s and 0.738  $\mu$ s). In line with the suggestions by Kumar et al. (2020) and Kook et al. (2017) we also tested removing the initial 1  $\mu$ s and 3  $\mu$ s, respectively. When using this approach, the number and decay time of the fitted lifetimes vary for each sample (Fig. 2). Removing initial channels from the fitted off-time data affects mostly the presence and lifetime of  $\tau_1$ .  $\tau_1$  is completely removed in samples FSM-3 and FSM-13LH. In

This is a **preprint** of the published article:

Riedesel, S., Jain, M., 2024. Excited state lifetime of electron trapping centres in alkali feldspars. *Radiation Measurements* 172, 107081. <https://doi.org/10.1016/j.radmeas.2024.107081>

samples FSM-7, FSM-11 and FSM-15  $\tau_1$  becomes slower until it is fully removed with sufficient exclusion of the initial off-time signal. The other two lifetimes are nearly unaffected in case of FSM-3, FSM-11, FSM-7 and FSM-15. For  $\tau_2$  and  $\tau_3$ , these samples experienced changes in lifetime dependent on the sample and lifetime. In case of FSM-13LH the removal of the initial 1  $\mu\text{s}$  results in  $\tau_2$  doubling compared to the measurement without signal removal. Removing the initial 3  $\mu\text{s}$  results in an increase of  $\tau_2$  from prior 1-2  $\mu\text{s}$  to over 8  $\mu\text{s}$ . Looking at these results, the approach of removing initial parts of the off-time signal might be questionable when investigating the time-resolved IRPL signals. However, for dating purposes removing the initial 1  $\mu\text{s}$ , as suggested by Kumar et al. (2020) will be a useful practicality, as this removes most of the laser breakthrough light, whilst still having sufficient off-time IRPL signal remaining for performing the dating procedure.

**Approach 3:** As a last test, we fixed  $\tau_1$  in all samples to 0.1  $\mu\text{s}$  (the value obtained for the laser breakthrough on an empty cup and material without IRPL<sub>880</sub> emission) while leaving the other two lifetimes free during the fitting procedure. When comparing the obtained lifetimes of  $\tau_2$  and  $\tau_3$  for the five samples we observe similar results to those obtained when all parameters are left free during the least square fitting approach (cf. Fig. 2).

We thus decided to use the approach of fixing  $\tau_1$  to 0.1  $\mu\text{s}$  for all further data analysis in the study because (i) it helps us in objectively removing the largest impact of the laser breakthrough, (ii) despite fixing the first lifetime we still obtain lifetimes for  $\tau_2$  and  $\tau_3$  close to the value obtained when fitting the entire off-time and leaving all fitting parameters free during the fitting procedure and (iii) it treats all samples equally, thus hopefully allowing an objective analysis of our results.

Since the breakthrough of the 830 nm laser is minimal for the IRPL<sub>955</sub> detection window, we decided to leave all lifetimes free to vary in the fitting approach of the IRPL<sub>955</sub> signal.

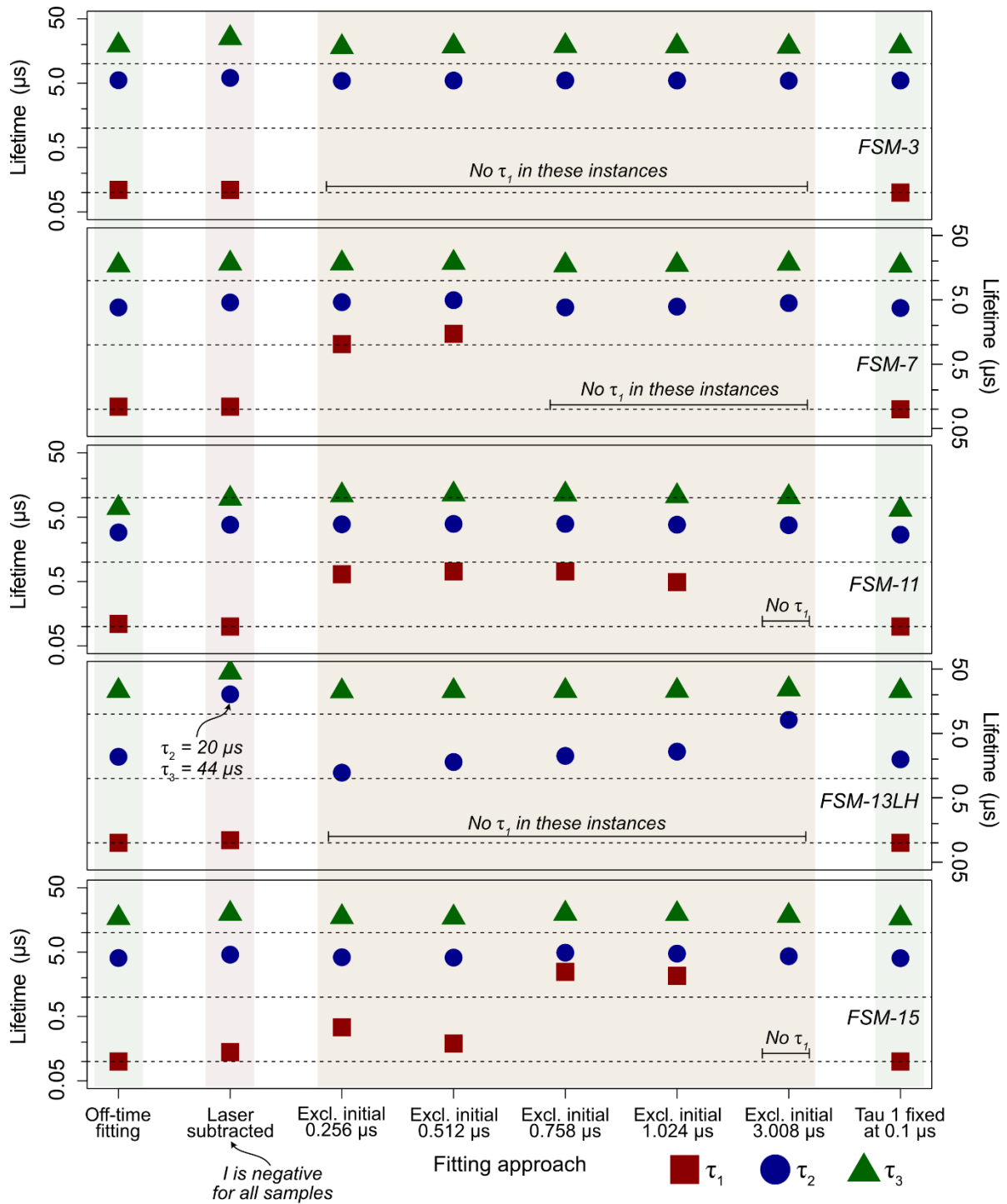


Fig. 2. To remove the influence of the laser signal on the IRPL<sub>880</sub> emission of the sample, different extraction methods were tested on aliquots from five different samples. "Off-time fitting" refers to fitting of the signal off-time, without any further modifications. For the "Laser subtracted" column the laser signal measured on an empty cup was subtracted from the signal recorded for the sample. For the steps referring to the exclusion of the initial signals, successive channels were removed from the initial off-time signal, aiming at isolating the signal, which is independent of the laser. As the last step, the first lifetime (τ<sub>1</sub>) was fixed to 0.1 μs for fitting, whilst the other two lifetimes were left to vary freely. Each point represents one aliquots of each sample.

### 3.2 On-time durations

During the on-time the signal rises gradually according to its characteristic lifetime; in the limiting case the signal reaches a steady state (plateau). This implies that the ratio of IRPL signal to the breakthrough will be a function of the on-time duration. Thus, in order to confirm the accuracy of our analysis, we test the influence of using different on-time duration on the lifetime measurements. For this experiment we used the protocol described in Table 2 on all eleven feldspar samples to test on-time durations of 5  $\mu$ s and 10  $\mu$ s against 20  $\mu$ s, as used in section 3.1. The breakthrough contamination relative to the signal will decrease systematically from 5  $\mu$ s to 20  $\mu$ s. The off-time decay was fitted using equation 1 and the sum of three exponential function, while fixing  $\tau_1$  to 0.1  $\mu$ s for the IRPL<sub>880</sub> signal.

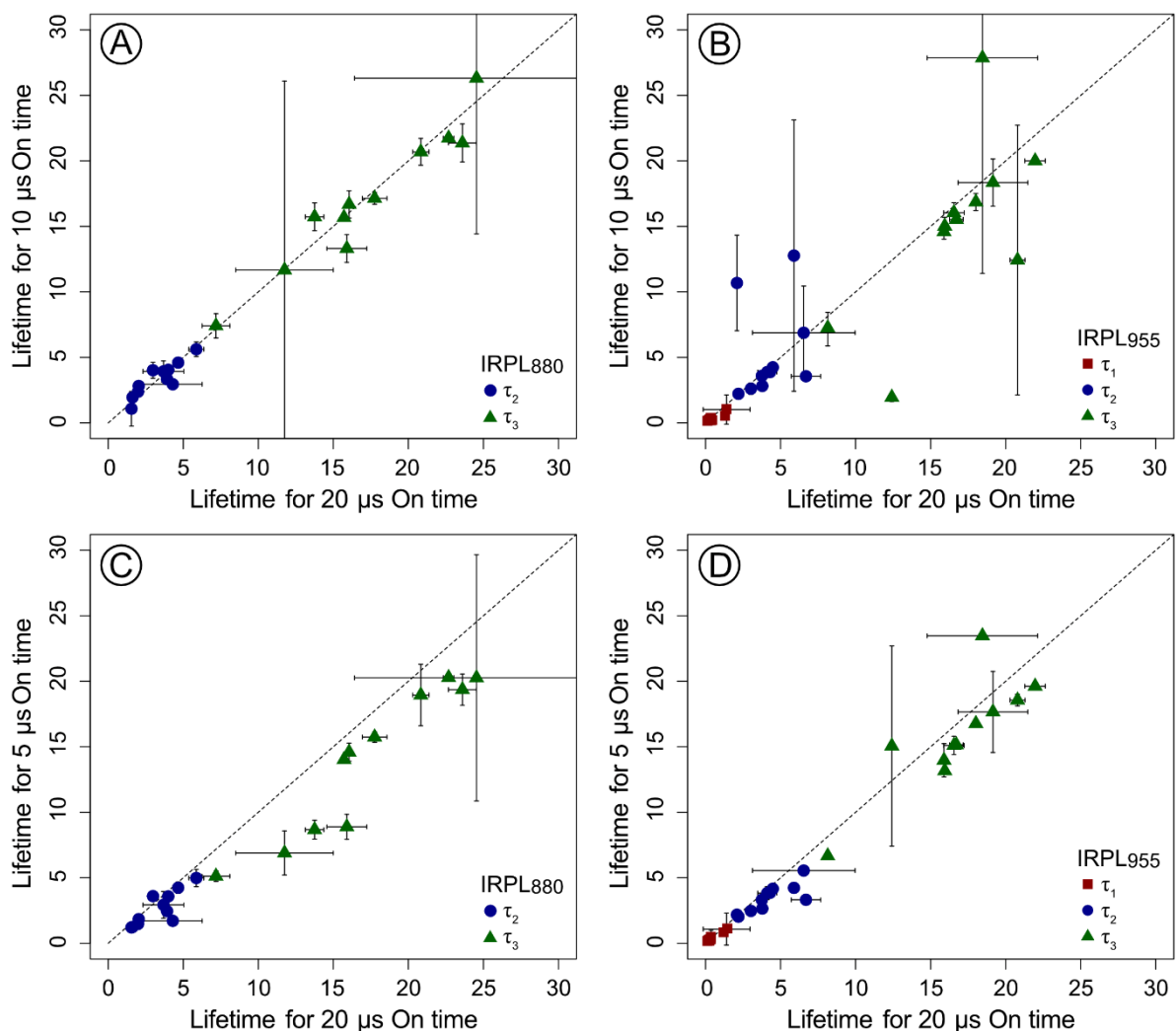


Fig. 3. Comparison of off-time lifetimes recorded after different durations of off-times. A) 20  $\mu$ s compared to 10  $\mu$ s for IRPL<sub>880</sub>. B) 20  $\mu$ s compared to 10  $\mu$ s for IRPL<sub>955</sub>. C) 20  $\mu$ s compared to 5  $\mu$ s for IRPL<sub>880</sub>. D) 20  $\mu$ s compared to 5  $\mu$ s IRPL<sub>955</sub>. Each data point is the average of two aliquots per sample and the standard deviation.

This is a **preprint** of the published article:

Riedesel, S., Jain, M., 2024. Excited state lifetime of electron trapping centres in alkali feldspars. *Radiation Measurements* 172, 107081. <https://doi.org/10.1016/j.radmeas.2024.107081>

Figure 3 shows the comparison of the fitted IRPL<sub>880</sub> (Fig. 3A,C) and IRPL<sub>955</sub> (Fig. 3B,D) lifetimes measured using different on-time durations. The dotted line represents the 1:1 line. The lifetimes derived from the 10  $\mu$ s on-time data are indistinguishable from those for 20  $\mu$ s data (Figure 3A,B). However, the 5  $\mu$ s data tends to under-estimate the latter (Figure 3C,D). This tendency is much stronger for IRPL<sub>880</sub> signal where we have much larger breakthrough. The larger scatter observed for the IRPL<sub>955</sub> data is presumably due to its lower intensity. Since a visible change in lifetimes can be obtained when decreasing the on-time from 20  $\mu$ s/10  $\mu$ s down to 5  $\mu$ s an on-time of 20  $\mu$ s is used in the further course of this study. An off-time of 80  $\mu$ s is sufficient in the case of all samples to reach a stable background level prior to the next stimulation pulse.

Based on the observations outlined in section 3.1 and 3.2, all measurements were done with an on-time of 20  $\mu$ s and an off-time of 80  $\mu$ s, and the fitting analysis included three exponential components, with the first component assigned a fixed lifetime of 0.1  $\mu$ s in case of IRPL<sub>880</sub>. In case of the IRPL<sub>955</sub> all lifetimes were kept free during fitting.

#### 4 Factors influencing the lifetimes of the IRPL signals

In the following we compare the IRPL<sub>880</sub> and IRPL<sub>955</sub> signal intensities and lifetimes (section 4.1). We then proceed to present and discuss the dependence of IRPL<sub>880</sub> and IRPL<sub>955</sub> lifetimes on the sample composition (section 4.2) and which effect pulse annealing (i.e. preheating) has on the excited state lifetimes (section 4.3).

##### 4.1 Comparison of IRPL<sub>880</sub> and IRPL<sub>955</sub> signals

Figure 4A shows a linear relationship between the off-time signal intensity of both IRPL signals, as has also been reported in previous work (Jain et al., 2020). The intensity of the laser breakthrough is indicated in Fig. 4A.

When comparing lifetimes between IRPL<sub>880</sub> and IRPL<sub>955</sub> signals for different samples, we observe that  $\tau_2$  is uncorrelated (Fig. 4B), whereas  $\tau_3$  shows a weak trend between the two IRPL signals (cf. Fig. 4C). However, a re-evaluation of the data shows that both albite specimen CLBR and Al-I and perthitic feldspar FSM-11 show very weak IRPL<sub>880</sub> signals. The poor sensitivity of CLBR confirms previous report by Riedesel et al. (2021a), and since Al-I is also a single-phase feldspar, similar behaviour to CLBR was expected, potentially suggesting that single-phase albite does not emit IRPL<sub>880</sub>. FSM-11 shows a sensitive IRPL<sub>955</sub> signal with exceptional lifetimes of < 10  $\mu$ s, however it shows a weak IRPL<sub>880</sub> signal hindering a comparison between the two signals. If one rejects these three samples based on their poor IRPL<sub>880</sub> sensitivity, and hence the possibility of significant contamination by the laser (highlighted in figure 4C), then a cluster of  $\tau_3$  values, broadly consistent with 1:1 line, can be found. These data

This is a **preprint** of the published article:

Riedesel, S., Jain, M., 2024. Excited state lifetime of electron trapping centres in alkali feldspars. *Radiation Measurements* 172, 107081. <https://doi.org/10.1016/j.radmeas.2024.107081>

suggest that both, the IRPL<sub>880</sub> and IRPL<sub>955</sub>, centres have a common lifetime of the dominant component of the IRPL signal, i.e. the slowest component ( $\tau_3$ ), in agreement with previous findings by Kumar et al. (2020).

All other samples show  $\tau_2$  and  $\tau_3$  lifetimes in defined ranges.  $\tau_2$  ranges from  $(1.99 \pm 0.06) \mu\text{s}$  (FSM-6LH) to  $(5.9 \pm 0.5) \mu\text{s}$  (FSM-3) for IRPL<sub>880</sub> and from  $(3.75 \pm 0.05) \mu\text{s}$  (FSM-15) to  $(6.69 \pm 0.98) \mu\text{s}$  (FSM-13LH) for IRPL<sub>955</sub>.  $\tau_3$  ranges from  $(15.71 \pm 0.05) \mu\text{s}$  to  $(24.5 \pm 8.1) \mu\text{s}$  for IRPL<sub>880</sub> and from  $(15.89 \pm 0.08) \mu\text{s}$  to  $(20.8 \pm 0.5) \mu\text{s}$  for IRPL<sub>955</sub>. Please note that these are the average ( $\pm$  standard deviation) of the two aliquots measured per sample. For illustration purposes we displayed the lifetimes measured for each aliquot in Fig. 5A and B. Another interesting observation is that for weakly luminescent samples we observe a small dependency of the lifetime on the intensity of the signal, which is more pronounced for the IRPL<sub>880</sub> signal than for the IRPL<sub>955</sub> signal (see Fig. S5 in the supplementary material). This suggests that the laser breakthrough impacts the lifetime measurements in case of the dimmer samples. However, since lifetimes measured for IRPL<sub>880</sub> and IRPL<sub>955</sub> emissions are similar in each sample (Fig. 4B, C), we still consider our results to be valid for most samples. We will, however, disregard the IRPL<sub>880</sub> results of albite specimen CLBR and Al-I due to the lack of an IRPL<sub>880</sub> emission. For FSM-11, although it shows only very weak IRPL<sub>880</sub> emission, the off-time decay is very different to the laser breakthrough (see Fig. S4I, J). Thus, we will still include this sample in our discussion.

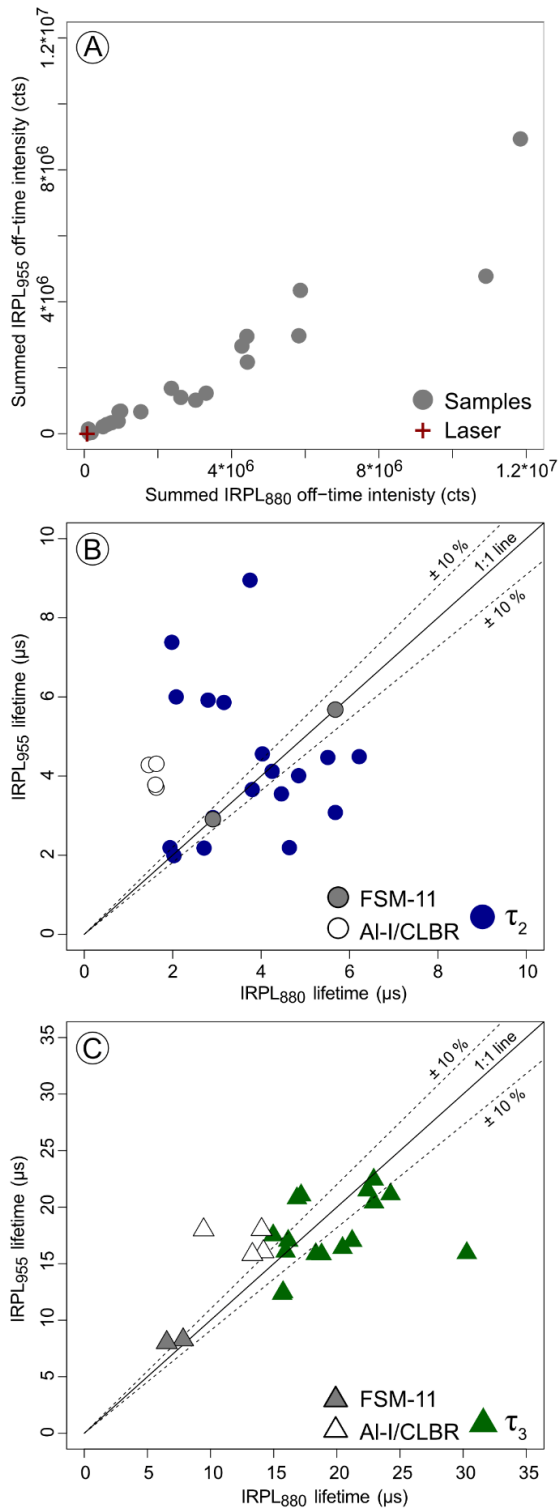


Fig. 4. (A) Comparison of the IRPL<sub>880</sub> and IRPL<sub>955</sub> signal intensities. For this plot the entire off-time signal for each emission was integrated. (B) Comparison of  $\tau_2$  for the off-time of IRPL<sub>880</sub> and IRPL<sub>955</sub>. (C) Comparison of  $\tau_3$  for the off-time of IRPL<sub>880</sub> and IRPL<sub>955</sub>. A one-to-one line and 10 % deviation from this line are indicated in B and C.

## 4.2 Influence of feldspar chemistry and structure on IRPL lifetimes

Here we explore potential effects of the sample chemistry and structural state on the IRPL lifetimes. To visualise the results, the samples and their recorded lifetimes were ranked according to the samples K-feldspar content (Fig. 5). The summed off-time intensity is displayed in Fig. 5A and B. Here the intensity of the individual aliquots measured per sample are shown. The relative integral contribution from each lifetime to the overall off-time signal is visualised in the size of the data points (Fig. 5C, D), where each data point represents the average of two aliquots. The numerical fitting results are given in Tables S1 and S2 for the IRPL<sub>880</sub> and IRPL<sub>955</sub> signals, respectively.

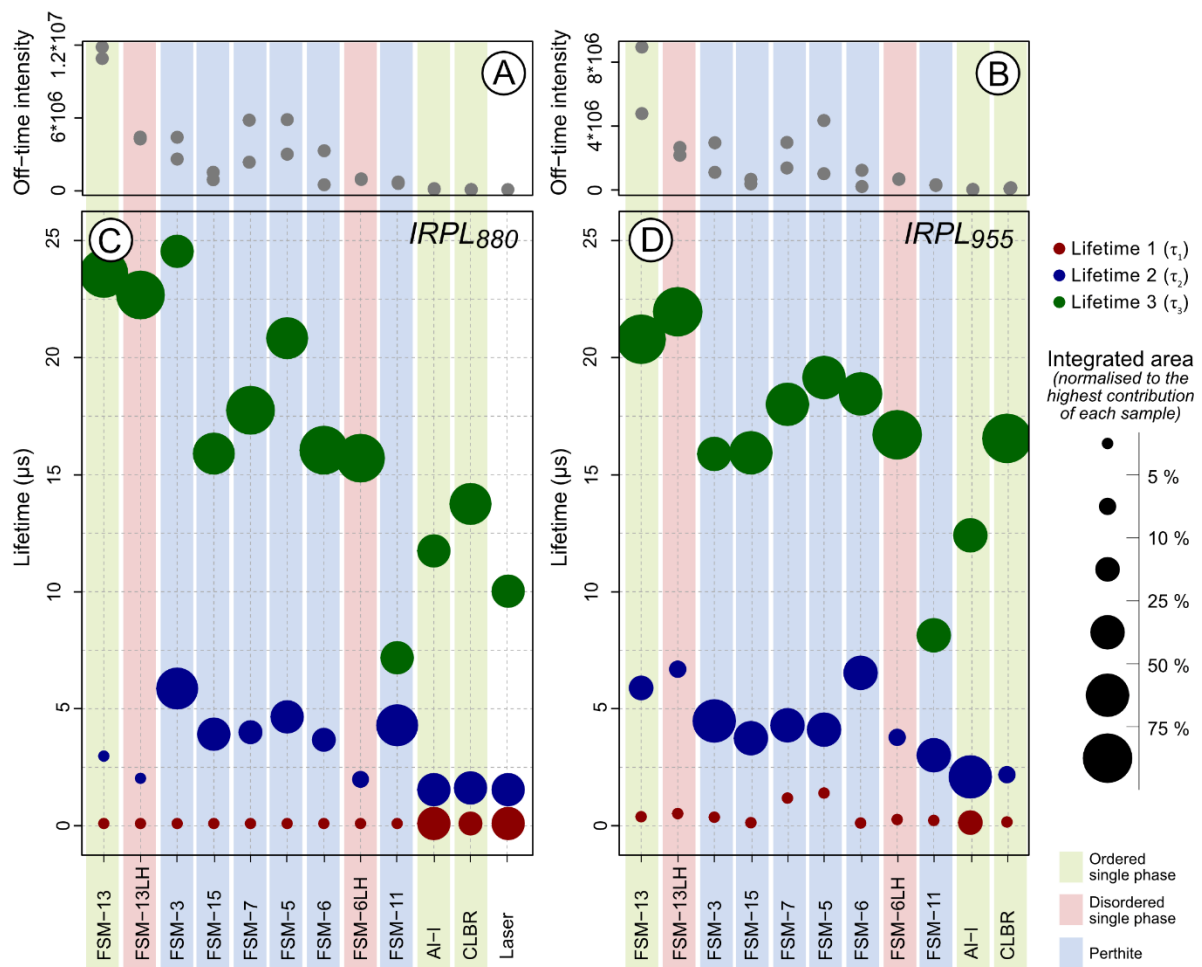


Fig. 5. Intensities of total integrated off-time signals for IRPL<sub>880</sub> (A) and IRPL<sub>955</sub> (B). Lifetimes obtained through fitting using the sum of three exponential functions for the IRPL<sub>880</sub> (C) and IRPL<sub>955</sub> signals (D). The results are ordered according to each sample's K-feldspar content (KFS, %). Each data point is the average of two aliquots per sample. Uncertainties are not displayed but can be taken from table S1 and S2 for IRPL<sub>880</sub> and IRPL<sub>955</sub>, respectively. The size of the points corresponds to the integrated area under the exponential function for each lifetime. The integrated area for each lifetime was normalised to total area, i.e. the sum of three exponentials, for each sample. Although the IRPL<sub>880</sub> data for Al-I and CLBR is disregarded for further discussion, we added the relative contributions of the three lifetimes to subfigure C for the sake of completeness.

### IRPL<sub>880</sub> lifetimes

Although  $\tau_1$  can be ignored in case of the IRPL<sub>880</sub> signal due to the breakthrough of the excitation laser, it is worth mentioning that  $\tau_1$  contributes to less than 5 % to the integrated off-time signal in most samples. The only exceptions are single-phase albite specimens Al-I and CLBR, where  $\tau_1$  contributes to 30 % and 20 % to the overall IRPL<sub>880</sub> off-time signal, respectively.

In the remaining nine alkali feldspar samples investigated,  $\tau_2$  shows lifetimes ranging from  $(1.99 \pm 0.06)$   $\mu\text{s}$  (FSM-6LH) to  $(5.9 \pm 0.5)$   $\mu\text{s}$  (FSM-3). The relative contribution of  $\tau_2$  to the overall off-time signal is sample-dependent: <2 % in samples FSM-13 and FSM-13LH, 7 % in FSM-6LH, 50 % in FSM-11 and 67 % in FSM-3. Samples with low  $\tau_2$  contribution (<7%) are single-phase feldspars, whereas perthites show higher contributions, with  $\tau_2$  even being the dominant lifetime in FSM-11 and FSM-3.

$\tau_3$  is the dominant lifetime component in most samples, with the exception of FSM-3 and FSM-11. In all other samples  $\tau_3$  contributes to at least 50 % to the overall signal. In samples FSM-13 and FSM-13LH  $\tau_3$  makes up nearly 100 % of the total off-time signal. Comparing  $\tau_3$  of all samples in relation to their K-feldspar content shows a trend of decreasing  $\tau_3$  lifetime with decreasing K-feldspar content of the sample (Fig. 5C). Please note that the samples are ordered according to their K-feldspar content. For the actual K-feldspar content please refer to Table 1.

### IRPL<sub>955</sub> lifetimes

For the IRPL<sub>955</sub> signal all three lifetimes can be investigated (Table S2, Fig. 5B). Here,  $\tau_1$  ranges from  $(0.14 \pm 0.01)$   $\mu\text{s}$  (single phase albite Al-I) to  $(1.4 \pm 1.6)$   $\mu\text{s}$  (macroperthite FSM-5), with FSM-5 and FSM-7 being the only samples exhibiting  $\tau_1$  lifetimes slower than 1  $\mu\text{s}$ . Similarly to IRPL<sub>880</sub>,  $\tau_1$  has the smallest contribution to the overall IRPL<sub>955</sub> off-time signal, making up less than 5 % of the total signal in all samples, except for single-phase albite Al-I. Here  $\tau_1$  contributes to ~20 % of the overall signal.

Lifetime  $\tau_2$  ranges from  $(2.09 \pm 0.14)$   $\mu\text{s}$  (single phase albite Al-I) to  $(6.69 \pm 0.98)$   $\mu\text{s}$  (disordered K-feldspar FSM-13LH). The contribution of  $\tau_2$  to the IRPL<sub>955</sub> off-time signal ranges from ~8 to ~9 % (disordered samples FSM-13LH and FSM-6LH, single-phase albite CLBR) to over 50 % (Al-I).  $\tau_2$  is the dominant lifetime in case of perthites FSM-3 (53 %) and FSM-11 (49 %) and single-phase albite Al-I (53 %).

Lifetime  $\tau_3$  ranges from  $(8.14 \pm 0.17)$   $\mu\text{s}$  (perthite FSM-11) to  $(21.96 \pm 0.68)$   $\mu\text{s}$  (disordered single-phase sample FSM-13LH). Only FSM-11 and single-phase albite Al-I ( $12.41 \pm 0.11$   $\mu\text{s}$ ) exhibit  $\tau_3$  lifetimes faster than 15  $\mu\text{s}$ . The longest lifetime is dominant in most samples but contributes to at least 28 % of the total signal in all samples.

A sample-to-sample comparison of the three different lifetimes obtained from fitting the IRPL<sub>955</sub> off-time signal, shows weak dependence of  $\tau_3$  on the sample's K-feldspar content. When comparing the ordered and disordered sample pairs no systematic effect, as visible for IRPL<sub>880</sub>, can be observed for the IRPL<sub>955</sub> signal. While disordering from FSM-13 to FSM-13LH led to an increase in  $\tau_2$  and  $\tau_3$  values, a decrease in these lifetimes was observed when disordering FSM-6 to FSM-6LH.

### 4.3 Effect of thermal detrapping on IRPL lifetimes

To test the thermal stability of the IRPL signals and to investigate potential dependencies of the lifetime on the depletion of the trapped charge population, we performed pulse annealing experiments (Table 3) on selected samples: the ordered/disordered sample pairs FSM-13 (single-phase microcline) and FSM-13LH (sanidine) and FSM-6 (perthite) and FSM-6LH (sanidine), as well as two perthites (FSM-3 and FSM-5).

The total sum of the off-time signal intensity shows a similar trend for both emissions (Figs. 6A and 6B), as also observed by Jain et al. (2020): A stable signal plateau is reached during the first measurement cycle (50 °C annealing temperature) and persists until a post irradiation annealing temperature of 400 °C. Following annealing temperatures >400 °C the IRPL<sub>880</sub> and IRPL<sub>955</sub> signal intensity decreases for most samples. In the two artificially disordered samples (FSM-13LH and FSM-6LH) the IRPL<sub>880</sub> and IRPL<sub>955</sub> signal intensities remain stable or a small increase in IRPL intensity between 400 and 450 °C can be observed, after which the signal decreases. However, the signal does not reach the initial intensity recorded prior to irradiation (cf. Fig. 6A, B). Interestingly, only pre-annealed (artificially disordered) feldspars show IRPL signals stable >400 °C.

To analyse potential changes to the off-time lifetimes of both IRPL signals due to preheating, the time-resolved signals for each pulse anneal step were fitted following the findings of section 3.1. The results for  $\tau_2$  and  $\tau_3$  of the IRPL<sub>880</sub> signal are shown in Fig. 6D and F and for all three lifetimes of the IRPL<sub>955</sub> signal in Fig. 6C, E and G. The data was normalised to the corresponding lifetime obtained from fitting the off-time signal after an annealing step at 50 °C. The red envelope curve represents the mean of all aliquots and the standard deviation and is displayed for the visualisation of overall trends in the data.

Investigating changes in off-time lifetimes with annealing temperature is challenging due to the scatter in the data (cf. Fig. 6C-G). On an average,  $\tau_1$  shows a small increase in lifetime with preheat temperature for IRPL<sub>955</sub>. For  $\tau_2$  and  $\tau_3$  of both IRPL signals an increasing spread in the data can be observed for annealing temperatures >400 °C. On average  $\tau_2$  decreases with increasing preheat temperature for both IRPL signals (Fig. 6D, E). This decreasing trend is visible for all samples, except for the pre-annealed samples FSM-13LH and FSM-6LH, where  $\tau_2$  remains constant in case of IRPL<sub>880</sub> (Fig. 6D). For IRPL<sub>955</sub> all samples show a decrease in  $\tau_2$  lifetime with increasing temperature (Fig. 6E). In contrast to  $\tau_2$  and

This is a **preprint** of the published article:

Riedesel, S., Jain, M., 2024. Excited state lifetime of electron trapping centres in alkali feldspars. *Radiation Measurements* 172, 107081. <https://doi.org/10.1016/j.radmeas.2024.107081>

similar to  $\tau_1$ , the longer lifetime component ( $\tau_3$ ) shows a slight increase as a function of preheat temperature for the IRPL<sub>955</sub> signal (cf. Fig. 6F, G) but it remains rather constant throughout the pulse annealing experiment for IRPL<sub>880</sub>. A steady decrease in  $\tau_3$  can only be observed for FSM-6, for both signals.

We associate the larger spread in the data at higher temperatures to a decrease in signal intensity, which affects the noise level (cf. Fig. 6A,B, cf. Ankjærgaard et al. 2010). We observe a similar dependence of  $\tau_2$  from individual samples (Figures 6 D,E) on preheat temperature, as was observed for their signal intensities (Figures 6A, B). Decreasing  $\tau_2$  lifetimes could indicate the impact of laser breakthrough light due to lower IRPL<sub>880</sub> signal intensities. However, since we observe faster  $\tau_2$  lifetimes for IRPL<sub>880</sub> and for IRPL<sub>955</sub>, where the latter is negligibly affected by breakthrough, we are confident that the observed decrease is real.

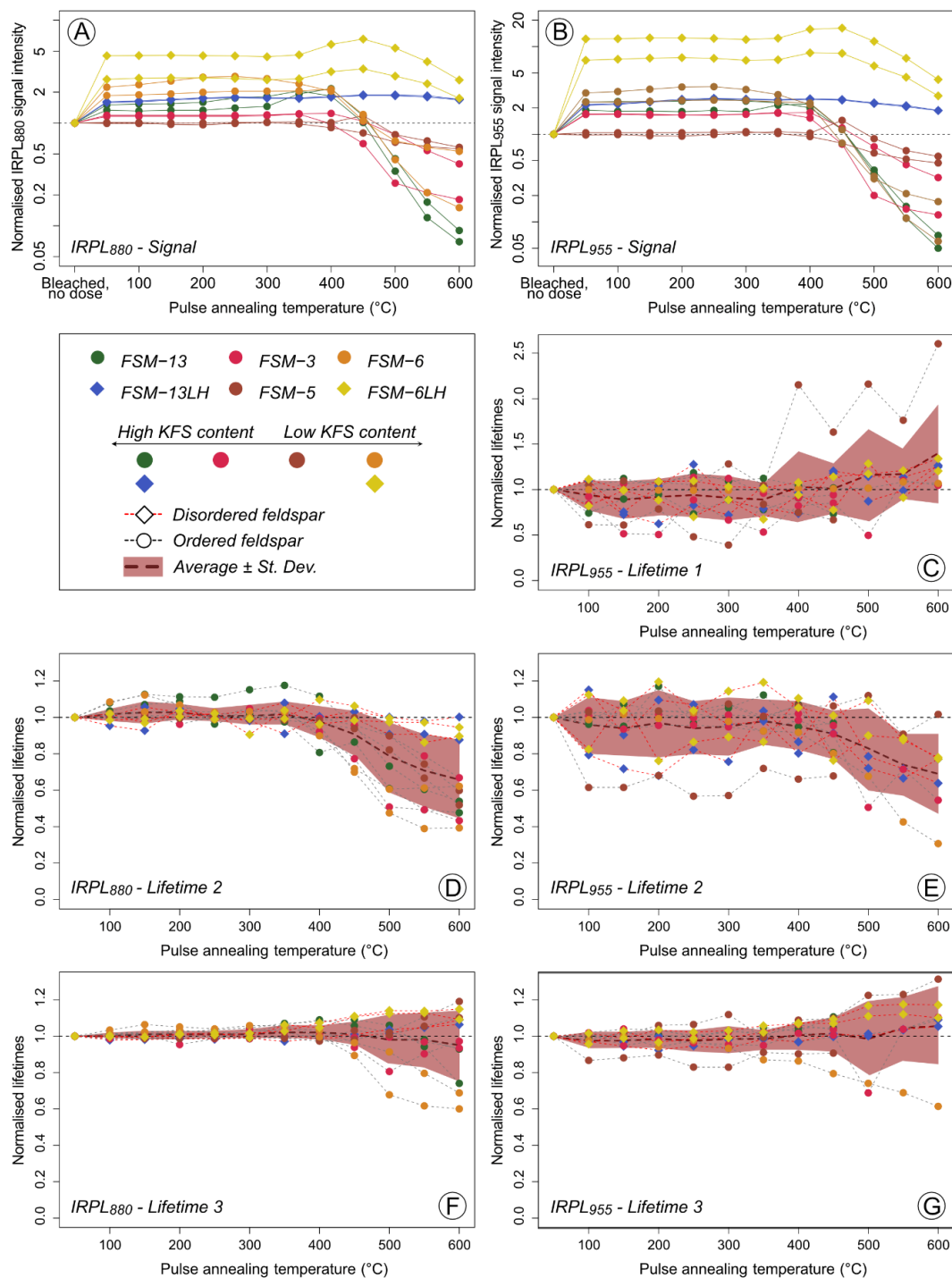


Fig. 6. Pulse annealing test to study the effect of high temperature pre-treatments on the time-resolved IRPL<sub>880</sub> and IRPL<sub>955</sub> off-time lifetimes. A), C), E) Pulse annealing experiment results for lifetimes 1 – 3 of IRPL<sub>955</sub>. B) and D) Pulse annealing experiment results for lifetimes 2 and 3 of IRPL<sub>880</sub>. For each sample two aliquots were measured, and the results of measured aliquots are displayed individually. The data is normalised to the lifetime measured after a preheat at 50 °C (first data point of the pulse annealing experiment). For A) and B) the entire off-time signal was integrated to obtain the sum, which was then normalised to the integrated off-time signal after a CW bleach at 290 °C, prior to administering a beta dose. The red envelope curves represent the mean of all aliquots and the standard deviation.

## 5 Discussion

### 5.1 Fitting and single exponential approximation

When fitting our time-resolved IRPL data a sum of three exponentials was chosen as this resulted in the smallest residuals. The first component ( $\tau_1$ ) of the IRPL<sub>880</sub> data represents the dominant part of the stimulation breakthrough, henceforth we discuss only two components in the IRPL<sub>880</sub> data and all three components in the IRPL<sub>955</sub> data.

The IRPL<sub>955</sub> data of Prasad et al. (2017) measured using an 885 nm laser, only shows a single exponential component with a lifetimes of  $\sim 40 \mu\text{s}$  (at 7 K) and  $\sim 30 \mu\text{s}$  (at 300 K), as would be expected for an intra-defect transition. Time-resolved measurements by Kumar et al. (2020) of both IRPL<sub>880</sub> and IRPL<sub>955</sub> stimulated using an 830 nm laser, show a slight deviation from a single exponential (cf. Figure 6 of Kumar et al., 2020). However, these authors approximated the decay using a single component. They estimated a lifetime of  $\sim 20 \mu\text{s}$  for both the signals. Our results using the same experimental configuration as Kumar et al. (2020), show similar results to their study with a dominant lifetime clustering around  $\sim 20 \mu\text{s}$ . For some of our samples (FSM-13, FSM-13LH, FSM-6LH and CLBR; cf. Figs. S6, S7, S9, S10, S11) we are also able to approximate this single exponential decay if the initial  $3 \mu\text{s}$  of the off-time are removed, resulting in lifetimes similar to those observed by Kumar et al. (2020).

Although, the contribution of  $\tau_1$  and  $\tau_2$  to the overall off-time signal is minor in most samples, it is instructive to explore potential sources of the deviation from the single exponential decay, as it would be expected for a simple intra-defect transition:

**Hypothesis 1:** A multiplicity of electron trapping centres emitting IRPL would result in a distribution of lifetimes. It has long been debated whether there exists multiple or a single type of electron trapping centres in feldspars (e.g. Clark and Sanderson, 1994; McKeever et al., 1997; Baril and Huntley, 2003; Murray et al., 2009; Jain and Ankjærgaard, 2011), with the single electron trapping centre type-model being favoured in the more recent literature (e.g. Andersen et al. 2012; Kumar et al., 2020). If there indeed are multiple types of trapping centres, then each of these could exhibit different excited state lifetimes, possibly accompanied with changes in emission wavelength, explaining the non-exponential curve observed here. However, the IRPL signals (IRPL<sub>880</sub> and IRPL<sub>955</sub>) are already thought to result from the same type of defect, but located in different lattice environments, causing the difference in emission wavelength (Kumar et al., 2020). This explanation requires that there is a similar distribution of both IRPL<sub>880</sub> and IRPL<sub>955</sub> centres, since they show similar components.

**Hypothesis 2:** The distance between the trapped electron and the nearest hole (i.e. Huntley, 2007; Jain et al., 2012) affects the lifetime because of changes to the local crystal field. However, if this were the

case one would expect a significant change in the emission wavelength as well. We lack enough information to estimate whether the range of expected wavelengths is consistent with the broad IRPL spectra measured for these samples (Riedesel et al., 2021a). While direct testing of this hypothesis requires a spectral time-resolved study, our pulse-anneal data to some extent eliminate this hypothesis. Increasing preheat temperature would gradually eliminate the proximal pairs by recombination (Jain et al, 2012; Jain et al., 2015); thus the relative signal contribution from different components should have changed with preheat. However, Figure S13 shows that the relative intensity of each component stays constant with preheat temperature.

**Hypothesis 3:** The non-exponential decay arises due to excitation to the band tail states. Our excitation light is of higher energy ( $\sim 1.49$  eV, 830 nm) than the IR resonance peak, based on IRPL spectra for these samples (Riedesel et al., 2021a), which is likely to significantly populate the band-tail states. Prasad et al. (2017) chose an 885 nm (1.4 eV) excitation laser, thus exciting slightly sub-resonance for their sample which showed an IRPL excitation peak at  $\sim 955$  nm (1.3 eV). It is thus likely that the participation of the band tail states give rise to other preferred leakage routes, in addition to the excited-to-ground state relaxation from the trap itself.

The longest lifetime ( $\tau_3$ ) observed is the dominant source of IRPL signal. We thus relate this lifetime to the excited state of the IRPL<sub>880</sub> and IRPL<sub>955</sub> electron trapping centres. We speculate that the observed faster lifetimes ( $\tau_1$  and  $\tau_2$ ) are a result of recombination of electrons from the band tail states to the ground state of the electron trap. We speculate that the two components ( $\tau_1$  and  $\tau_2$ ), is just a convenient mathematical description of an overall non-exponential decay route due to a distribution in the energies of band tail states. A decrease in  $\tau_2$  with preheat temperature (see Fig. 6D, E), could then result from leakage of band tail states to other empty traps that increase in concentration with the preheat temperature (e.g. due to thermal eviction of recombination). This model, does not imply that the relative contribution of different components will change with preheat, as is consistent with Figure S13.

The nearest-neighbour recombination model (Jain et al., 2012) predicts a slight increase in the excited state lifetime of the main trap, i.e.,  $\tau_3$ , with an increase in the recombination distance because of the corresponding decrease in the probability of tunnelling from the excited state. Thus, the decrease in the leakage probability from the excited state should decrease the overall lifetime of the excited state measured through IRPL; this is consistent with the slight increasing trend of  $\tau_3$  in the IRPL<sub>955</sub> signal. Note that IRPL<sub>955</sub> trapping centres are more affected by nearest-neighbour recombination centres in comparison to the IRPL<sub>880</sub> trapping centres (Jain et al. 2020). A thorough testing of this hypothesis requires time-resolved measurements at different temperatures using different laser wavelengths.

## 5.2 Dependencies of measured lifetimes

For our eleven chemically and structurally different alkali feldspars tested we observed a decreasing trend in  $\tau_3$  lifetime with decreasing K-feldspar content. This trend is more pronounced in IRPL<sub>880</sub> compared to IRPL<sub>955</sub>. In feldspars, cations are located in cavities within the framework. In alkali feldspars this is either K<sup>+</sup> or Na<sup>+</sup>, with K<sup>+</sup> having a significantly larger ionic radius than Na<sup>+</sup>. The ionic radius of the cation influences bond lengths and framework, with the framework collapsing around the smaller Na<sup>+</sup> ion. This chemically and structurally induced variation in the crystal could potentially explain the trend in measured  $\tau_3$  lifetimes with decreasing K-feldspar content. Overall, the lifetimes are rather consistent across the range of alkali feldspars measured, ranging from 16  $\mu$ s to 25  $\mu$ s (when the dimmest samples are excluded), and thus indicating the same type of defect. A similar consistency was observed in trap depths measurements performed by Kars et al. (2014), Riedesel et al. (2019, 2021a), and Kumar et al. (2020). Due to the similarities in trap depth for the feldspars measured, Riedesel et al. (2019) suggested that the defect acting as electron trapping site in feldspars is located on the framework.

## 5.3 IRPL compared to IRSL lifetimes

IRSL in feldspars is understood as the result from electron-hole recombination (cf. Jain and Ankjærsgaard, 2011). Lifetimes obtained for IRSL range mostly from < 1  $\mu$ s to ~ 20  $\mu$ s (e.g. Clark et al., 1997; Tsukamoto et al., 2006; Riedesel et al., 2023), with some slower lifetimes being recorded (e.g. Ankjærsgaard et al., 2009; Ankjærsgaard and Jain, 2020; Riedesel et al., 2023). The excited state lifetimes ( $\tau_3$ ) measured here using time-resolved IRPL, are of the orders of tens of microseconds, which is long enough to allow tunnelling recombination from the excited states, or leakage to the band tail states, giving rise to the IRSL signals on relatively shorter time scales.

## 6 Conclusions

In this paper we performed time-resolved infrared photoluminescence (IRPL) measurements to constrain excited state lifetimes in IRPL emitting electron trapping centres in chemically and structurally different feldspars. We observed a non-exponential time-resolved IRPL decay, which we mathematically resolve into three exponentially decaying components. The fastest lifetime is contaminated by laser breakthrough in case of IRPL<sub>880</sub> signal. We suggest that the slowest yet most dominant component  $\tau_3$  with a cluster of lifetimes between 15-25  $\mu$ s represent the excited state lifetime of the electron trapping centres investigated. We hypothesise that the faster two lifetimes of the IRPL<sub>955</sub> signal and at least  $\tau_2$  of the time-resolved IRPL<sub>880</sub> signal arise due to a transition from the band-tail states. Our results on changes in IRPL lifetimes with preheat temperature are broadly

This is a **preprint** of the published article:

Riedesel, S., Jain, M., 2024. Excited state lifetime of electron trapping centres in alkali feldspars. *Radiation Measurements* 172, 107081. <https://doi.org/10.1016/j.radmeas.2024.107081>

consistent with this model and imply a competition in alternative recombination (leakage) routes from the excited state and the band tail states.

Comparing IRPL lifetimes with published IRSL lifetimes suggests that electron-hole recombination occurs on time scales faster than the excited-to ground-state relaxation within the electron trap. Thus, recombination is possible through leakage from the excited state, as has been proposed in the recent literature.

## **Acknowledgements**

We would like to thank Myungho Kook (DTU) for technical support during the time-resolved IRPL measurements and Anthony M.T. Bell for performing the XRF and XRD measurements. We would like to thank our colleagues who provided some of the samples used in this study: Jan-Pieter Buylaert (DTU, Denmark) for FSM-13, Geoff A.T. Duller (Aberystwyth University, United Kingdom) for FSM-6 and Adrian A. Finch (University of St. Andrews, United Kingdom) for CLBR. SR acknowledges funding by the European Union's Horizon Europe research and innovation programme under the Marie Skłodowska-Curie grant agreement (RECREATE, grant number 101103587) during writing of the manuscript. MJ acknowledges funding by the European Union (ERC, LUMIN, project number 101097215) during writing of the manuscript. Views and opinions expressed are however those of the author(s) only and do not necessarily reflect those of the European Union or the European Research Council Executive Agency. Neither the European Union nor the granting authority can be held responsible for them. We would like to thank an anonymous reviewer and the editor Dr Eduardo Yukihiro for their constructive comments, which helped us to improve the manuscript.

## **References**

- Andersen, M. T., Jain, M., Tidemand-Lichtenberg, P., 2012. Red-IR stimulated luminescence in K-feldspar: Single or multiple trap origin? *Journal of Applied Physics* 112, 1–11.
- Ankjærgaard, C., Jain, M., Kalchgruber, R., Lapp, T., Klein, D., McKeever, S.W.S., Murray, A.S., Morthekai, P., 2009. Further investigations into pulsed optically stimulated luminescence from feldspars using blue and green light. *Radiation Measurements* 44, 576-581.
- Ankjærgaard, C., Jain, M., 2010. Optically stimulated phosphorescence in orthoclase feldspar over the millisecond to second time scale. *Journal of Luminescence* 130, 2346-2355.
- Ankjærgaard, C., Jain, M., Hansen, P.C. and Nielsen, H.B., 2010. Towards multi-exponential analysis in optically stimulated luminescence. *Journal of Physics D: Applied Physics*, 43(19), 195501.

*This is a preprint of the published article:*

Riedesel, S., Jain, M., 2024. Excited state lifetime of electron trapping centres in alkali feldspars. *Radiation Measurements* 172, 107081. <https://doi.org/10.1016/j.radmeas.2024.107081>

Baril, M. R., Huntley, D. J., 2003. Optical excitation spectra of trapped electrons in irradiated feldspars. *Journal of Physics: Condensed Matter* 15, 8011–8027.

Bates, D.M., DebRoy, S., 2018. nls function—nonlinear least squares. R Core Team and contributors worldwide. The R stats package version 3.5.0.

Cassadanne, J.P., Roditi, M., 1996. The location, geology and mineralogy of gem tourmalines in Brazil. *Journal of Gemmology* 25 (4), 263–298.

Chithambo, M.L., 2003. Dependence of the thermal influence on luminescence lifetimes from quartz on the duration of optical stimulations. *Radiation Measurements* 37, 167–175.

Clark, R.J., Sanderson, D.C.W., 1994. Photostimulated luminescence excitation of spectroscopy of feldspars and micas. *Radiation Measurements* 23, 641–646. Clark, R.J., Bailiff, I.K., Tooley, M.J., 1997. A preliminary study of time-resolved luminescence in some feldspars. *Radiation Measurements* 27, 211–220.

Clark, R.J., Bailiff, I.K., 1998. Fast time-resolved luminescence emission spectroscopy in some feldspars. *Radiation Measurements* 29, 553–560.

Cunningham, G.J., 1981. Petrology and Geochemistry of Lewisian Pegmatites and Granites, N.W., Scotland. PhD thesis. Imperial Collage London, United Kingdom.

Deer, W.A., Howie, R.A., Zussman, J., 2013. An Introduction to the Rock-Forming minerals, third ed. Mineralogical Society of Great Britain and Ireland.

Demas, J.N., 1983. Excited State Lifetime Measurements. New York, London, Academic Press, 273 p.

Govindaraju, K., 1995. Update (1984-1995) on two GIT-IWG geochemical reference samples: albite from Italy, Al-I and iron formation sample from Greenland, IF-G. *Geostandards Newsletter* 19, 55–96.

Huntley, D.J., Lamothe, M., 2001. Ubiquity of anomalous fading in K-feldspars and the measurement and correction for it in optical dating. *Canadian Journal of Earth Sciences* 38, 1093–1106.

Hütt, G., Jaek, I., Tchonka, J., 1988. Optical Dating: K-feldspars optical response stimulation spectra. *Quaternary Science Reviews* 7, 381-385.

Jain, M., Ankjærgaard, C., 2011. Towards a non-fading signal in feldspar: Insight into charge transport and tunnelling from time-resolved optically stimulated luminescence. *Radiation Measurements* 46, 292-309. doi:10.1016/j.radmeas.2010.12.004

This is a **preprint** of the published article:

Riedesel, S., Jain, M., 2024. Excited state lifetime of electron trapping centres in alkali feldspars. *Radiation Measurements* 172, 107081. <https://doi.org/10.1016/j.radmeas.2024.107081>

Jain, M., Guralnik, B., Thalbitzer Andersen, M., 2012. Stimulated luminescence emission from localized recombination in randomly distributed defects. *Journal of Physics: Condensed Matter* 24, 385402. doi:10.1088/0953-8984/24/38/385402

Jain, M., Kumar, R., Kook, M., 2020. A novel coupled RPL/OSL system to understand the dynamics of the metastable states. *Scientific Reports* 10, 15565. <https://doi.org/10.1038/s41598-020-72434-4>

Kars, R.H., Wallinga, J., Cohen, K.M., 2008. A new approach towards anomalous fading correction for feldspar IRSL dating – tests on samples in field saturation. *Radiation Measurements* 43, 786–790.

Kars, R.H., Poolton, N.R.J., Jain, M., Ankjærgaard, C., Dorenbos, P., Wallinga, J., 2013. On the trap depth of the IR-sensitive trap in Na- and K-feldspar. *Radiation Measurements* 59, 103-113. <http://dx.doi.org/10.1016/j.radmeas.2013.05.002>

Kook, M., Kumar, R., Murray, A.S., Thomsen, K.J., Jain, M., 2017. Instrumentation for the non-destructive optical measurement of trapped electrons in feldspar. *Radiation Measurement* 120, 247-252. <https://doi.org/10.1016/j.radmeas.2018.06.001>

Kumar, R., Kook, M., Murray, A.S., Jain, M., 2018. Towards direct measurement of electrons in metastable states in K-feldspar: Do infrared-photoluminescence and radioluminescence probe the same trap? *Radiation Measurements* 120, 7-13. <https://doi.org/10.1016/j.radmeas.2018.06.018>

Kumar, R., Kook, M., Jain, M., 2020. Understanding the metastable states in K-Na aluminosilicates using novel site-selective excitation-emission spectroscopy. *Journal of Physics D: Applied Physics* 53, 465301. <https://doi.org/10.1088/1361-6463/aba788>

Kumar, R., Kook, M., Jain, M., 2021. Sediment dating using Infrared Photoluminescence. *Quaternary Geochronology* 62, 101147. <https://doi.org/10.1016/j.quageo.2020.101147>

Lapp, T., Jain, M., Ankjærgaard, C., Pritzel, L., 2009. Development of pulsed stimulation and Photon Timer attachments to the Risø TL/OSL reader. *Radiation Measurements* 44, 571-575. doi:10.1016/j.radmeas.2009.01.012

Li, B., Li, S.H., 2011. Luminescence dating of K-feldspar from sediments: A protocol without anomalous fading correction. *Quaternary Geochronology* 6, 468-479. doi:10.1016/j.quageo.2011.05.001

McKeever, S. W. S., Bøtter-Jensen, L., Agersnap Larsen, N., Duller, G. A. T., 1997. Temperature dependence of OSL decay curves: Experimental and theoretical aspects. *Radiation Measurements* 27 (2), 161–170.

*This is a preprint of the published article:*

Riedesel, S., Jain, M., 2024. Excited state lifetime of electron trapping centres in alkali feldspars. *Radiation Measurements* 172, 107081. <https://doi.org/10.1016/j.radmeas.2024.107081>

Murray, A. S., Buylaert, J. P., Thomsen, K. J., Jain, M., 2009. The effect of preheating on the IRSL signal from feldspar. *Radiation Measurements* 44, 554–559.

Pagonis, V., Morthekai, P., Singhvi, A.K., Thomas, J., Balaram, V., Kitis, G., Chen, R., 2012. Time-resolved infrared stimulated luminescence signals in feldspars: Analysis based on exponential and stretched exponential functions. *Journal of Luminescence* 132, 2330-2340. <https://doi.org/10.1016/j.jlumin.2012.04.020>

Prasad, A.K., Poolton, N.R.J., Kook, M., Jain, M., 2017. Optical dating in a new light: A direct, non-destructive probe of trapped electrons. *Scientific Reports* 7: 12097. <https://doi.org/10.1038/s41598-017-10174-8>

Riedesel, S., King, G.E., Prasad, A.K., Kumar, R., Finch, A.A., Jain, M., 2019. Optical determination of the width of the band-tail states, and the excited and ground state energies of the principal dosimetric trap in feldspar. *Radiation Measurements* 125, 40-51.

Riedesel, S., 2020. Exploring variability in the luminescence properties of feldspars. PhD Thesis Aberystwyth University.

Riedesel, S., Kumar, R., Duller, G.A.T., Roberts, H.M., Bell, A.M.T., Jain, M., 2021a. Site-selective characterisation of electron trapping centres in relation to chemistry, structural state and mineral phases present in singly crystal alkali feldspars. *Journal of Physics D: Applied Physics* 54, 385107.

Riedesel, S., Bell, A.M.T., Duller, G.A.T., Finch, A.A., Jain, M., King, G.E., Pearce, N.J., Roberts, H.M., 2021b. Exploring sources of variation in thermoluminescence emissions and anomalous fading in alkali feldspars. *Radiation Measurements* 141, 106541.

Riedesel, S., Duller, G.A.T., Ankjærgaard, 2023. Time-resolved infrared stimulated luminescence of the blue and yellow-green emissions – Insights into charge recombination in chemically and structurally different alkali feldspars. *Journal of Luminescence* 257, 119724. Doi: [10.1016/j.jlumin.2023.119724](https://doi.org/10.1016/j.jlumin.2023.119724)

Sanderson, D.C.W., Clark, R.J., 1994. Pulsed photostimulated luminescence of alkali feldspars. *Radiation Measurements* 23, 633-639.

Schlag, E.W., Schneider, S., Fischer, S.F., 1971. Lifetimes in excited states. *Annual Review of Physical Chemistry* 22, 465-526.

Thiel, C., Buylaert, J.-P., Murray, A.S., Terhorst, B., Hofer, I., Tsukamoto, S., Frechen, M., 2011. Luminescence dating of the Stratzing loess profile (Austria) – Testing the potential of an elevated temperature post-IR IRSL protocol. *Quaternary International* 234, 23-31. doi:10.1016/j.quaint.2010.05.018

This is a **preprint** of the published article:

Riedesel, S., Jain, M., 2024. Excited state lifetime of electron trapping centres in alkali feldspars. *Radiation Measurements* 172, 107081. <https://doi.org/10.1016/j.radmeas.2024.107081>

Thomsen, K.J., Murray, A.S, Jain, M., Bøtter-Jensen, L., 2008. Laboratory fading rates of various luminescence signals from feldspar-rich sediment extracts. *Radiation Measurements* 43, 1474-1486. doi:10.1016/j.radmeas.2008.06.002

Tsukamoto, S., Denby, P.M., Murray, A.S., Bøtter-Jensen, L., 2006. Time-resolved luminescence from feldspars: new insights into fading., *Radiation Measurements* 41, 790–795.

Ussher, W.A.E., Barrow, G., McAlister, D.A., 1909. The Geology of the Country Around Bodmin and St. Austell. *Memoirs of the Geological Survey England and Wales – Explanation of Sheet 347.*

Visocekas, R., 1985. Tunnelling radiative recombination on labradorite: its association with anomalous fading of thermoluminescence. *Nuclear Tracks and Radiation Measurements* 10, 521–529.

Wintle, A.G., 1973. Anomalous fading of thermoluminescence in mineral samples. *Nature* 245, 143–144.

## Excited state lifetime of electron trapping centres in alkali feldspars Supplementary Material

Svenja Riedesel<sup>a,b</sup> and Mayank Jain<sup>a</sup>

<sup>a</sup>Radiation Physics Division, Department of Physics, Technical University of Denmark, Risø Campus, Roskilde, Denmark

<sup>b</sup>Institute of Geography, University of Cologne, Cologne, Germany

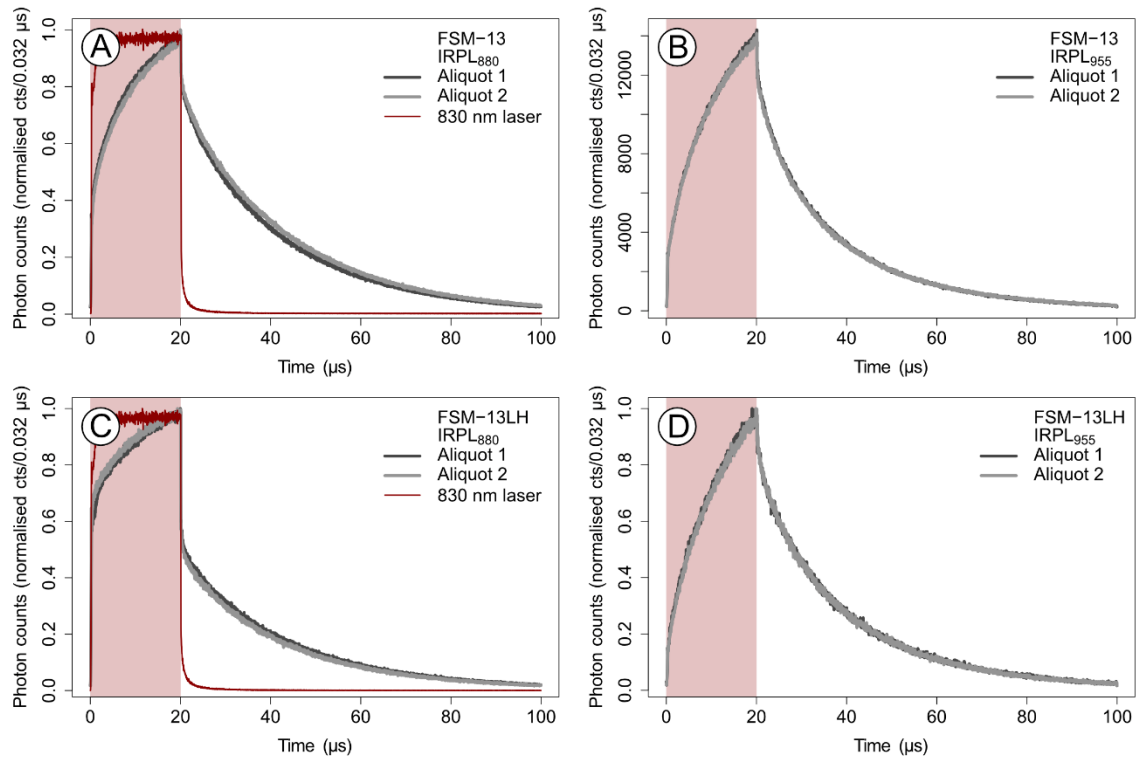


**Fig. S1.** A) Time-resolved IRPL<sub>880</sub> signal of single-phase microcline sample FSM-13, B) time resolved IRPL<sub>955</sub> of single-phase microcline sample FSM-13, C) time-resolved IRPL<sub>880</sub> signal of artificially disordered sample FSM-13LH, D) time-resolved IRPL<sub>955</sub> signal of artificially disordered sample FSM-13LH. The on-time is highlighted with the shaded rectangle.

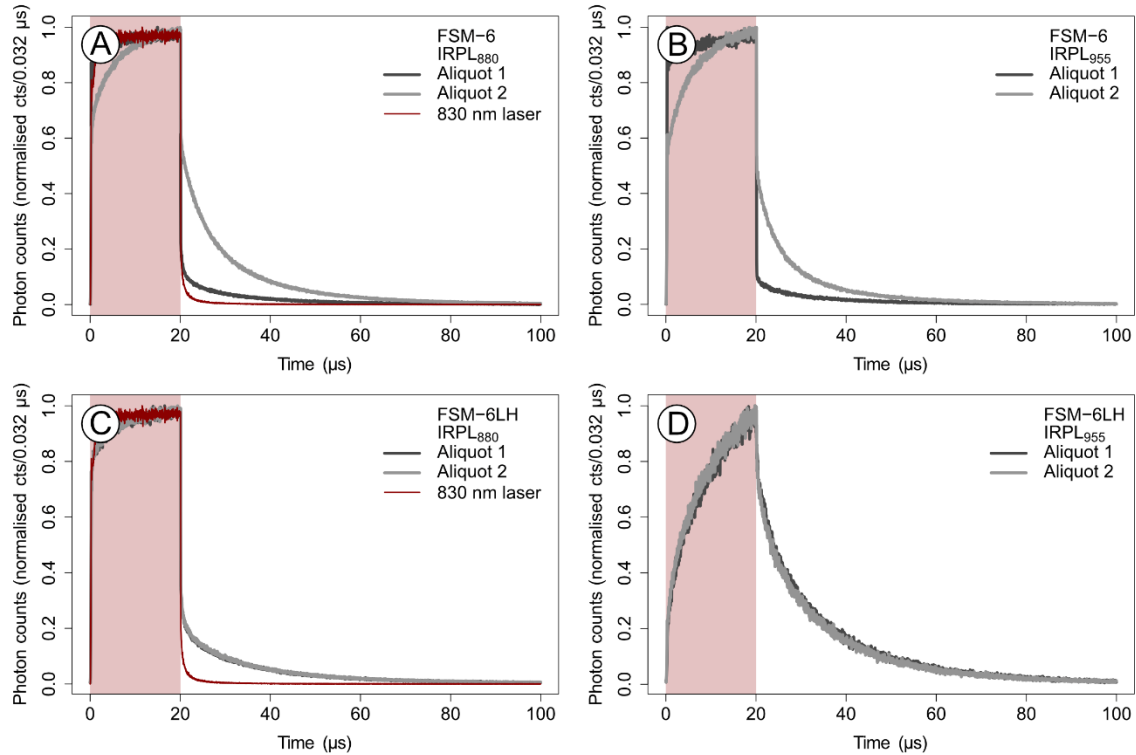


Fig. S2. A) Time-resolved IRPL<sub>880</sub> signal of perthite FSM-6, B) time resolved IRPL<sub>955</sub> of perthite FSM-6, C) time-resolved IRPL<sub>880</sub> signal of artificially disordered sample FSM-6LH, D) time-resolved IRPL<sub>955</sub> signal of artificially disordered sample FSM-6LH. The on-time is highlighted with the shaded rectangle.

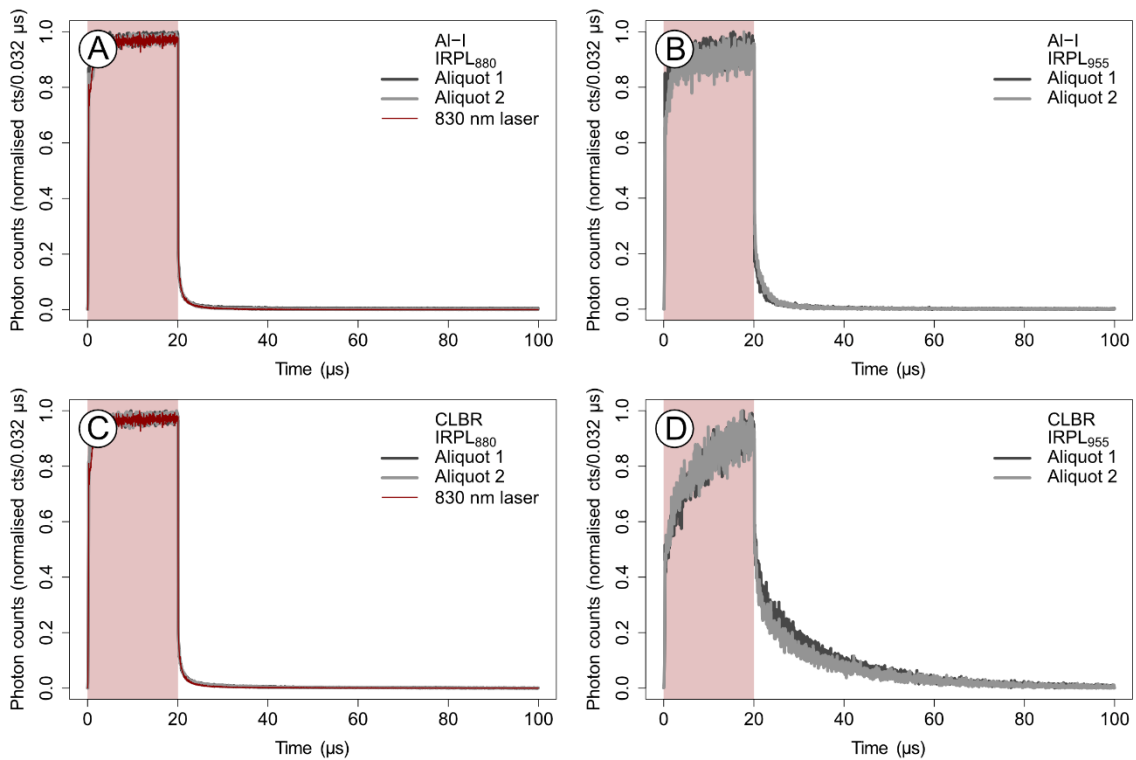


Fig. S3. Time-resolved IRPL<sub>880</sub> signal of single-phase samples AI-I (A) and CLBR (C), time resolved IRPL<sub>955</sub> of single-phase samples AI-I (B) and CLBR (D). The on-time is highlighted with the shaded rectangle.

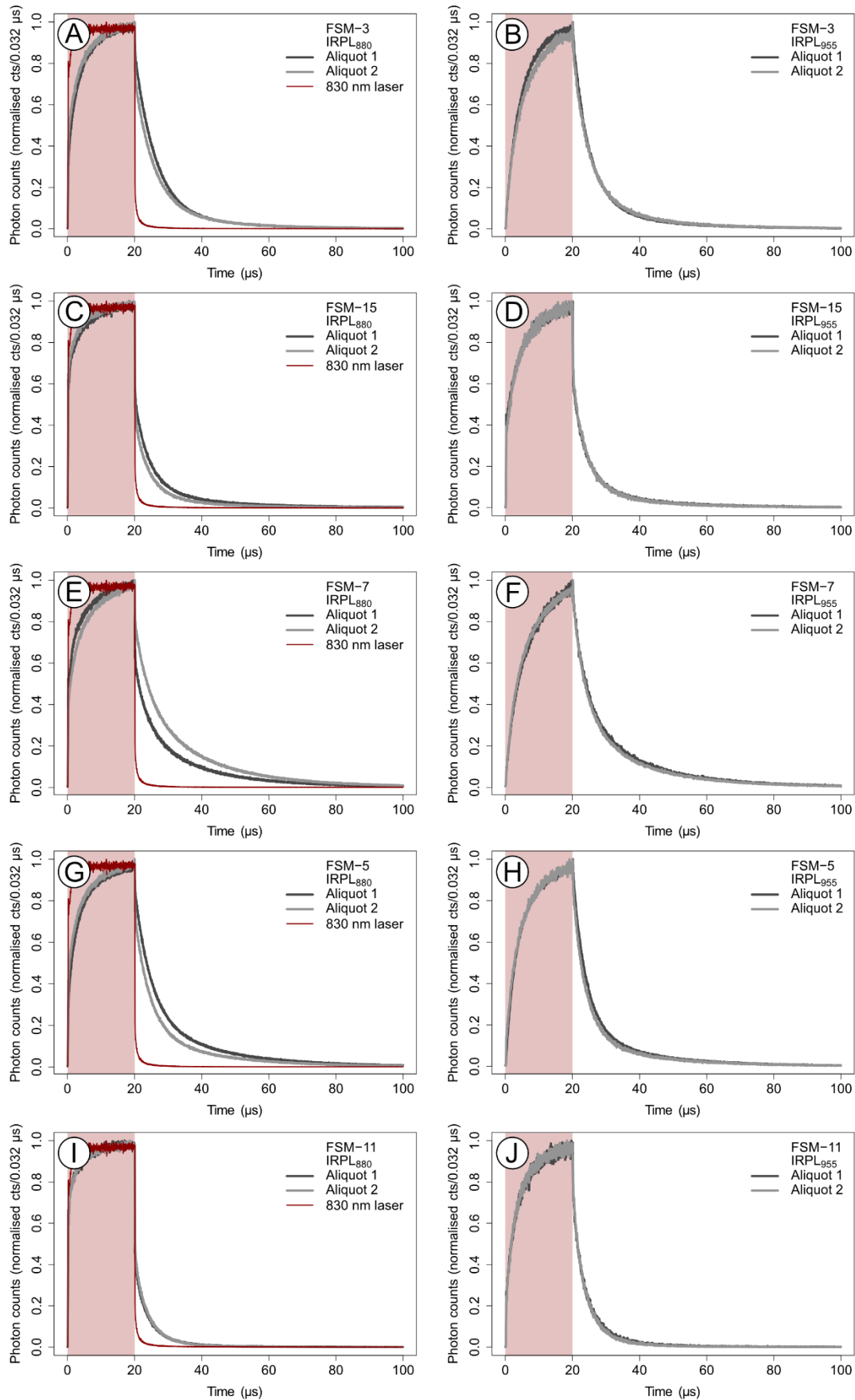


Fig. S4. Time-resolved IRPL<sub>880</sub> and IRPL<sub>955</sub> signals, respectively, for perthitic samples FSM-3 (A and B), FSM-15 (C and D), FSM-7 (E and F), FSM-5 (G and H) and FSM-11 (I and J).

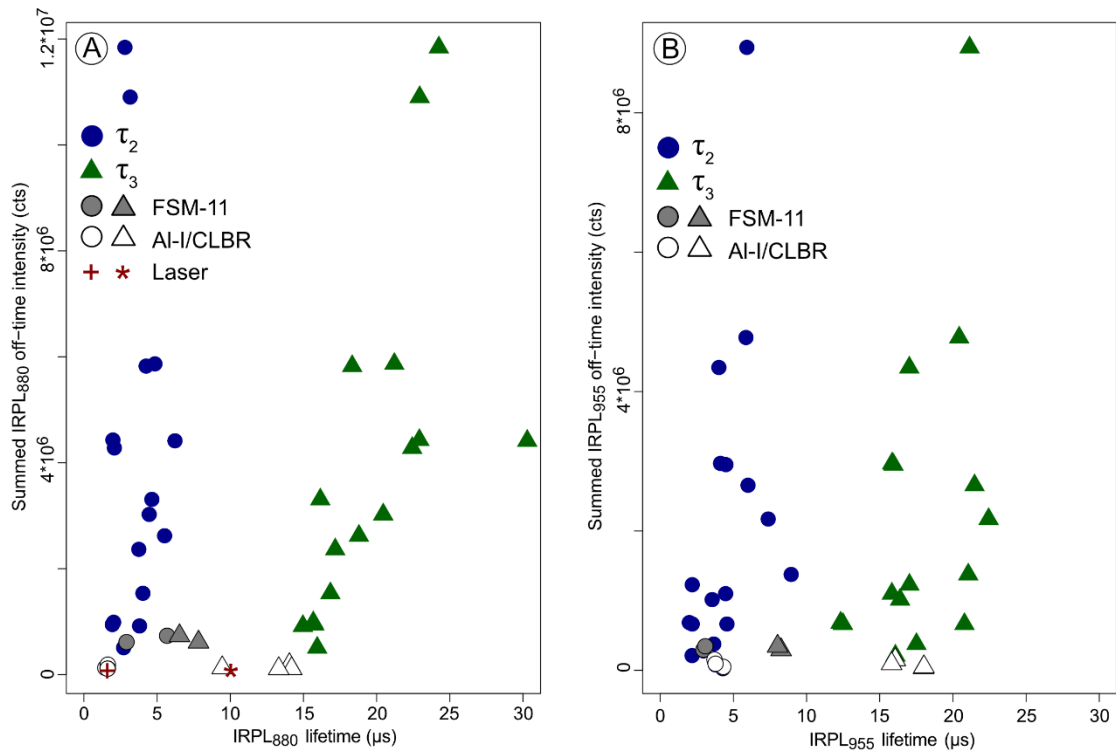


Fig. S5. A)  $IRPL_{880}$  intensity compared to the fitted lifetimes. B)  $IRPL_{955}$  intensity compared to the fitted lifetimes. The signal and lifetime of the laser off-time signal measured on an empty cup is display as a comparison.

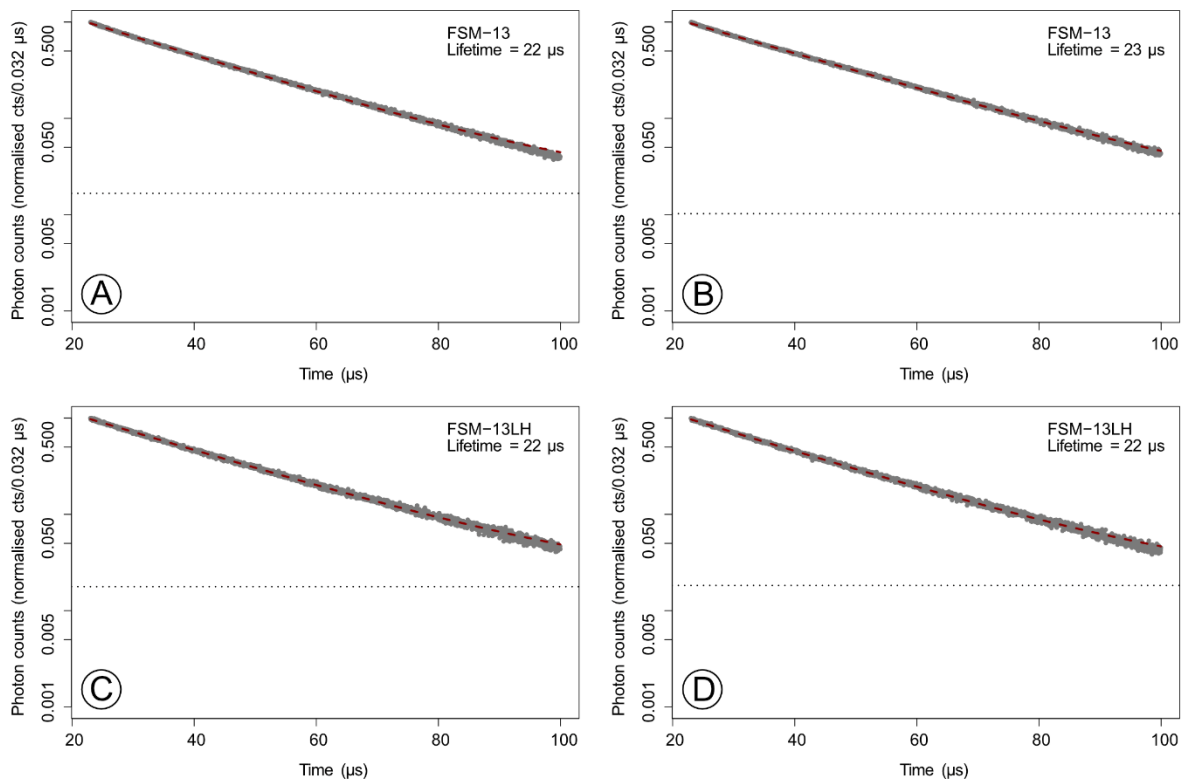


Fig. S6.  $IRPL_{880}$  off-time signal excluding the initial 3  $\mu s$  fitted using a single exponential function to enable a comparison with the data published by Kumar et al. (2020). The data is displayed for two aliquots of samples FSM-13 (A, B) and FSM-13LH (C, D).

This is a **preprint** of the published article:

Riedesel, S., Jain, M., 2024. Excited state lifetime of electron trapping centres in alkali feldspars. *Radiation Measurements* 172, 107081. <https://doi.org/10.1016/j.radmeas.2024.107081>

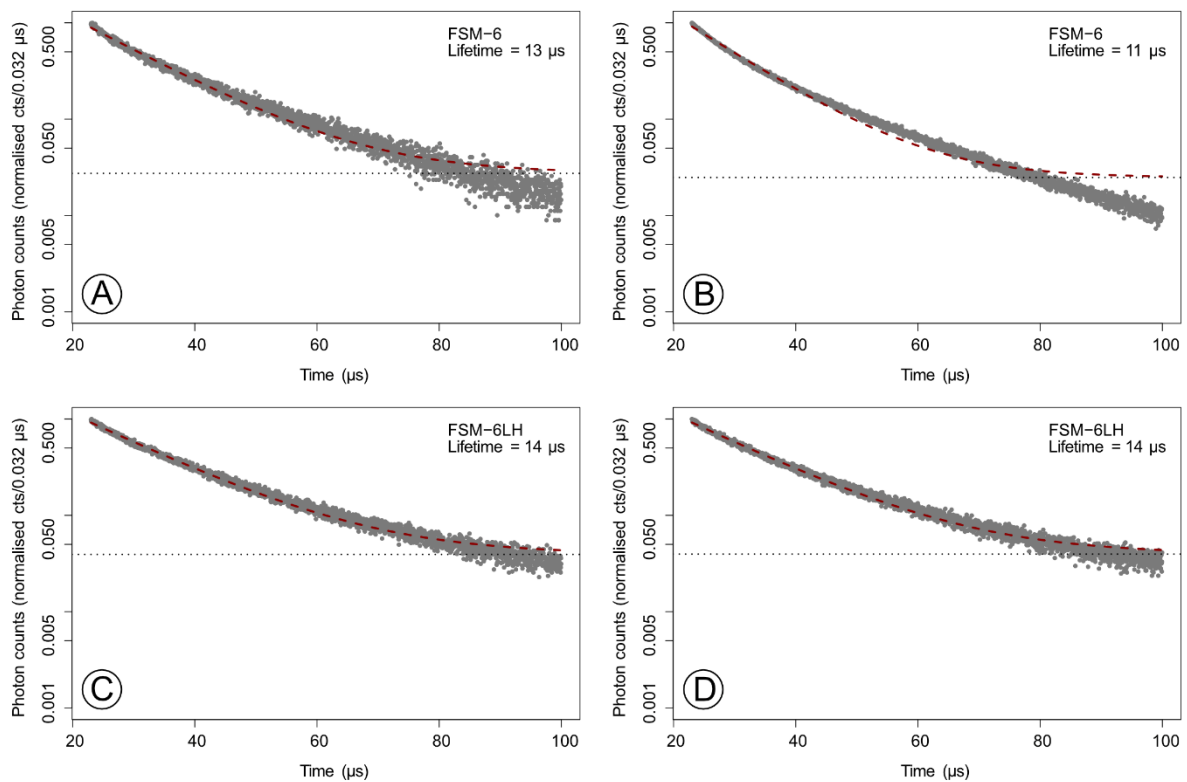


Fig. S7. IRPL<sub>880</sub> off-time signal excluding the initial 3 μs fitted using a single exponential function to enable a comparison with the data published by Kumar et al. (2020). The data is displayed for two aliquots of samples FSM-6 (A, B) and FSM-6LH (C, D).

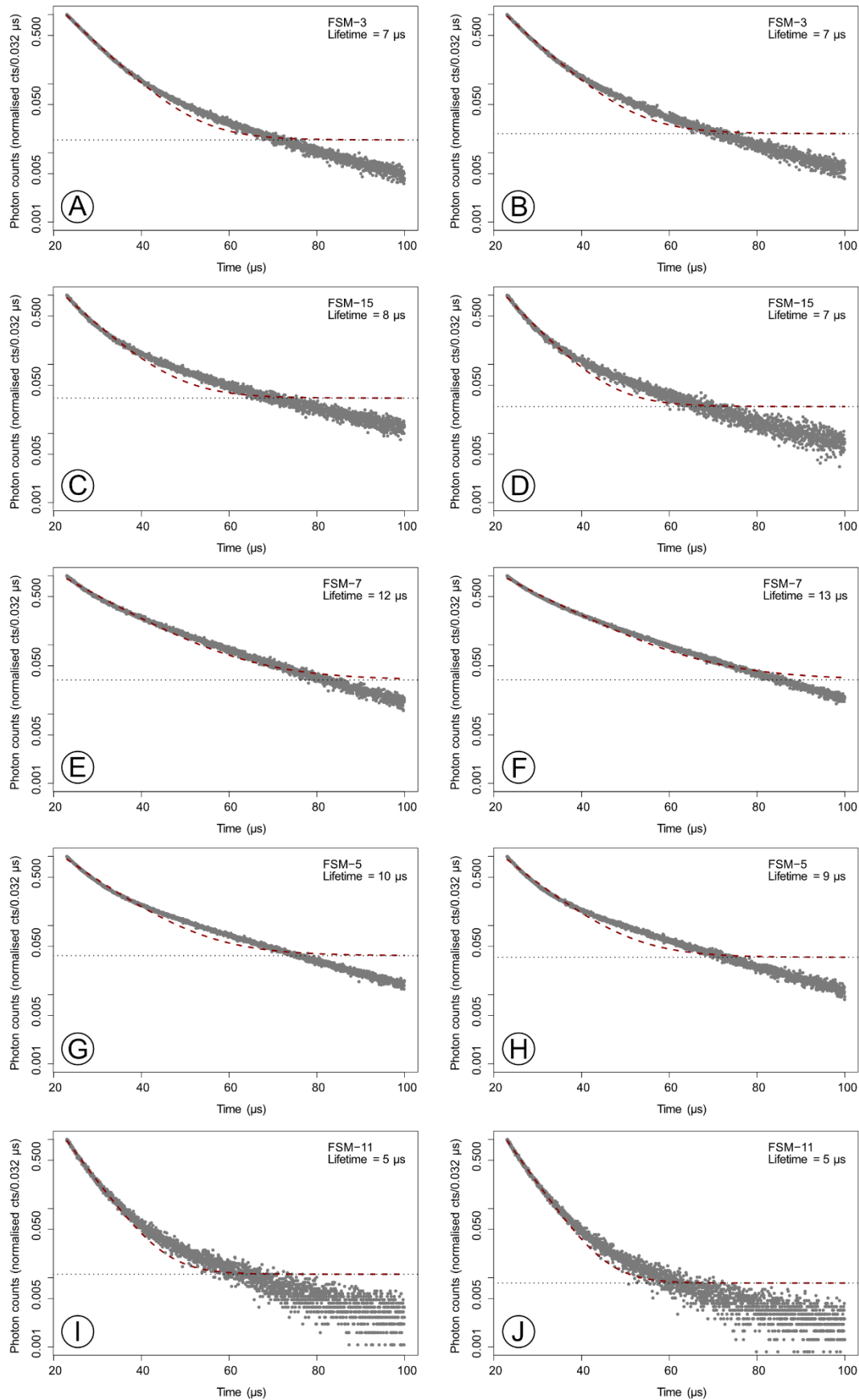


Fig. S8. IRPL<sub>880</sub> off-time signal excluding the initial 3  $\mu\text{s}$  fitted using a single exponential function to enable a comparison with the data published by Kumar et al. (2020). The data is displayed for two aliquots of perthitic samples FSM-3 (A, B), FSM-15 (C, D), FSM-7 (E, F), FSM-5 (G, H) and FSM-11 (I, J).

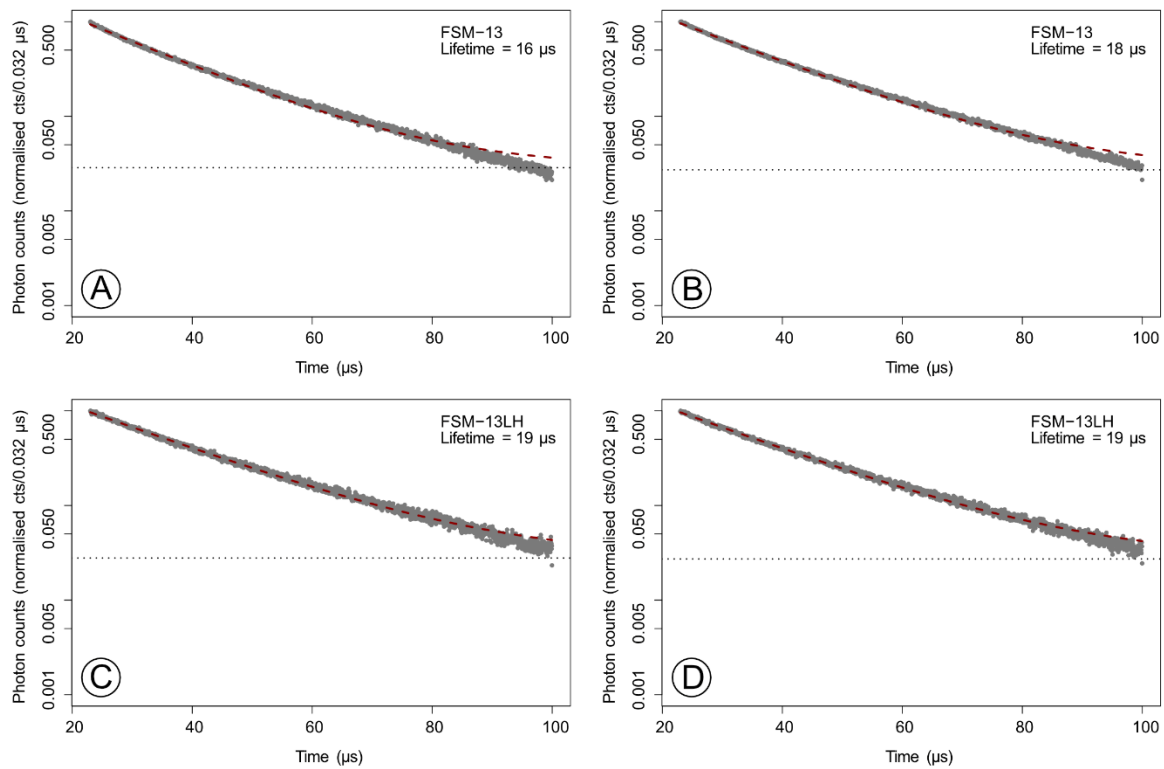


Fig. S9. IRPL<sub>955</sub> off-time signal excluding the initial 3 μs fitted using a single exponential function to enable a comparison with the data published by Kumar et al. (2020). The data is displayed for two aliquots of samples FSM-13 (A, B) and FSM-13LH (C, D).

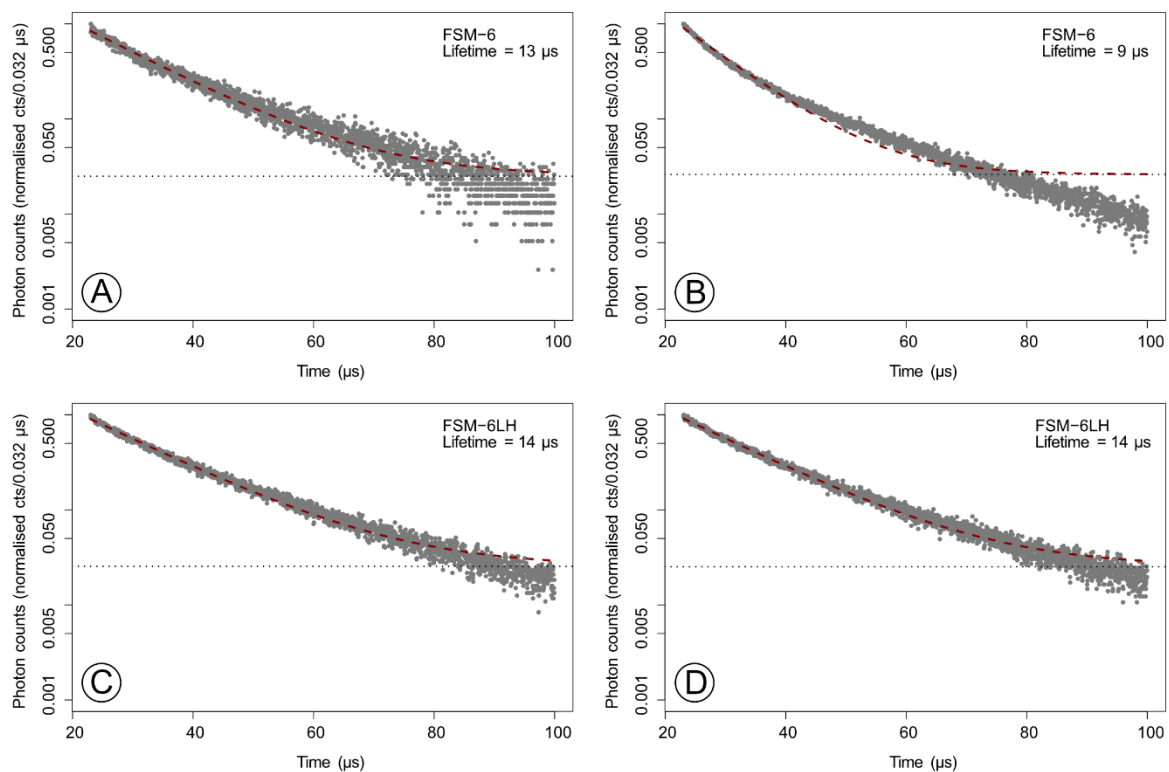


Fig. S10. IRPL<sub>955</sub> off-time signal excluding the initial 3 μs fitted using a single exponential function to enable a comparison with the data published by Kumar et al. (2020). The data is displayed for two aliquots of samples FSM-6 (A, B) and FSM-6LH (C, D).

This is a **preprint** of the published article:

Riedesel, S., Jain, M., 2024. Excited state lifetime of electron trapping centres in alkali feldspars. *Radiation Measurements* 172, 107081. <https://doi.org/10.1016/j.radmeas.2024.107081>

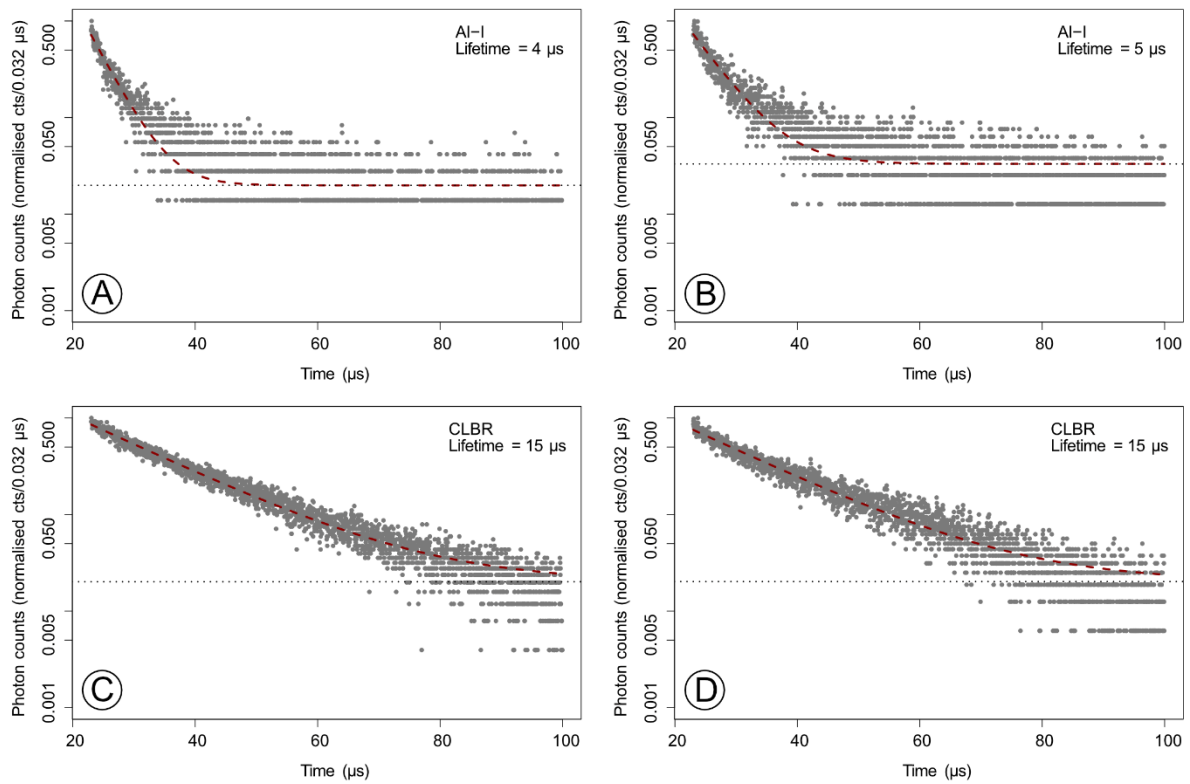


Fig. S11. IRPL<sub>955</sub> off-time signal excluding the initial 3 μs fitted using a single exponential function to enable a comparison with the data published by Kumar et al. (2020). The data is displayed for two aliquots of samples Al-I (A, B) and CLBR (C, D).

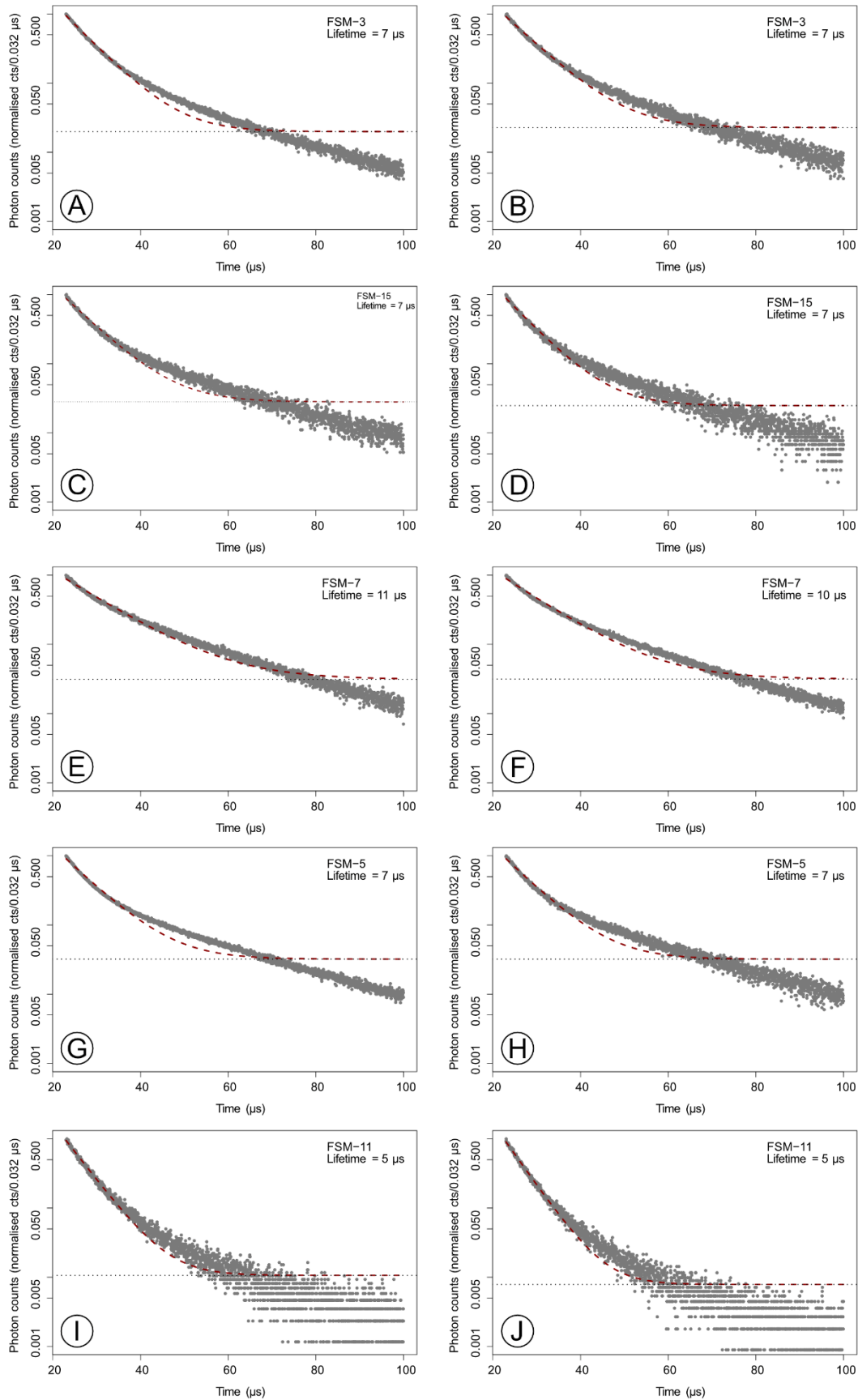


Fig. S12. IRPL<sub>955</sub> off-time signal excluding the initial 3  $\mu$ s fitted using a single exponential function to enable a comparison with the data published by Kumar et al. (2020). The data is displayed for two aliquots of perthitic samples FSM-3 (A, B), FSM-15 (C, D), FSM-7 (E, F), FSM-5 (G, H) and FSM-11 (I, J).

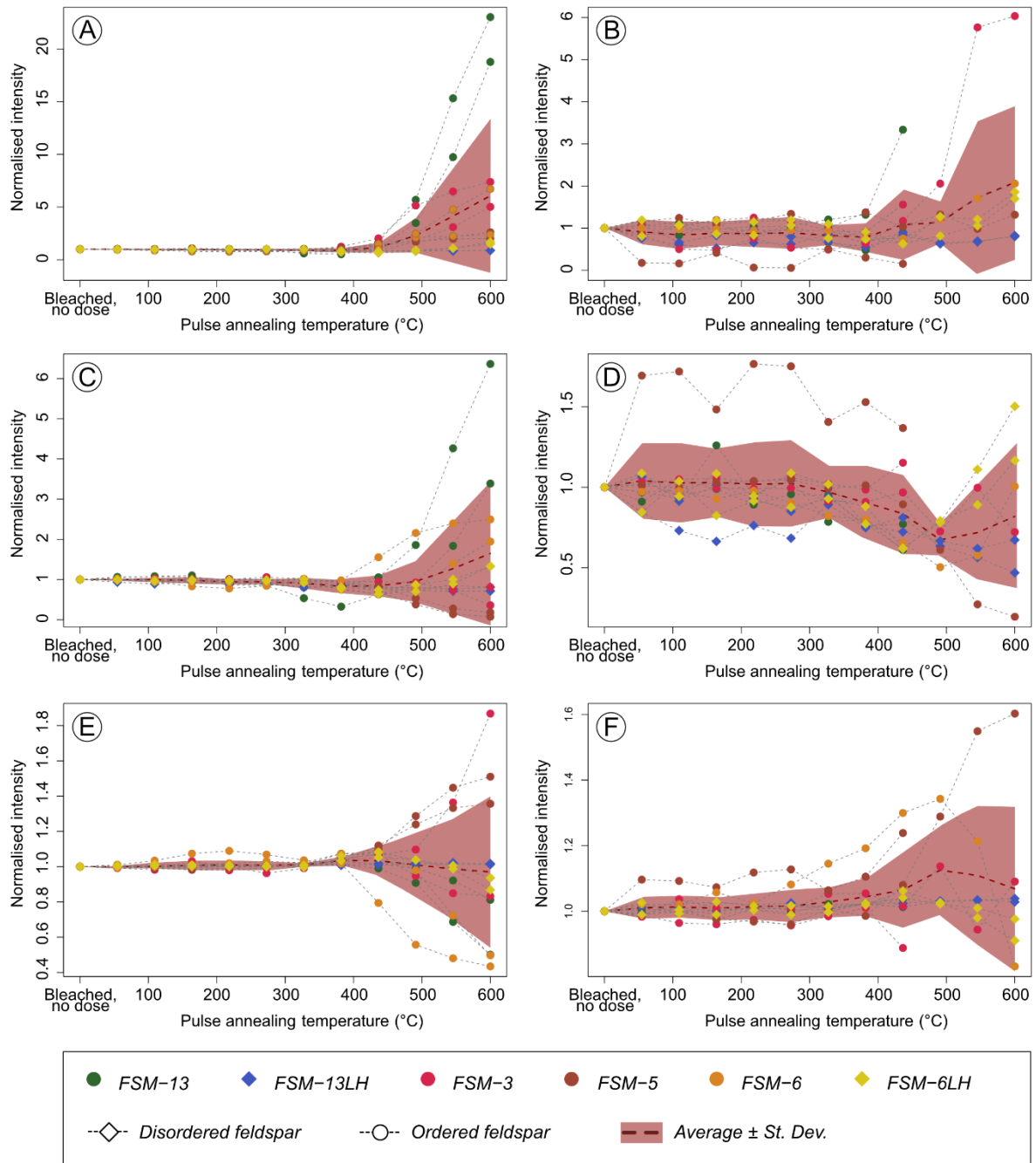


Fig. S13. Normalised relative intensities of the three lifetimes fitted to the time-resolved pulse anneal data. To obtain the data points, the relative contributions of each lifetime component's intensity were calculated, and the obtained results normalised to the first data point (bleached, no dose).

1 Table S1. IRPL<sub>880</sub> lifetimes obtained for all samples investigated by fitting the off-time decay of the IRPL<sub>880</sub> with the sum of three exponential functions, with the first lifetime being  
 2 fixed to 0.1  $\mu$ s. The values in the table are the average and standard deviation of two aliquots, which were measured per sample.  $I$  represents the intensity of each component,  $\tau$   
 3 the lifetime and  $A$  the amplitude (integrated area under the fitted curve). The different components are denoted using an index number. Prior to fitting the signals were normalised  
 4 to the last data point of the on-time. \*The small contribution of  $\tau_2$  and  $\tau_3$  for samples CLBR and AI-I shows that these samples basically show no IRPL<sub>880</sub> emission and that the signal  
 5 consists of the laser breakthrough only (see also Fig. 1 for details). We thus exclude the IRPL<sub>880</sub> results of AI-I and CLBR from our discussions.

Sample ID	KFS [%]	$I_1$	$\tau_1$ [ $\mu$ s]	$A_1$ [%]	$I_2$	$\tau_2$ [ $\mu$ s]	$A_2$ [%]	$I_3$	$\tau_3$ [ $\mu$ s]	$A_3$ [%]
<b>FSM-13</b>	98.5	0.21 $\pm$ 0.01	0.10	0.12 $\pm$ 0.02	0.09 $\pm$ 0.10	2.98 $\pm$ 0.25	1.64 $\pm$ 0.37	0.73 $\pm$ 0.02	23.60 $\pm$ 0.9	98.24 $\pm$ 0.38
<b>FSM-13LH</b>	98.5	0.56 $\pm$ 0.02	0.10	0.52 $\pm$ 0.04	0.06 $\pm$ 0.06	2.03 $\pm$ 0.07	1.15 $\pm$ 0.09	0.46 $\pm$ 0.01	22.68 $\pm$ 0.35	98.33 $\pm$ 0.13
<b>FSM-3</b>	82.5	0.24 $\pm$ 0.10	0.10	0.40 $\pm$ 0.21	0.62 $\pm$ 0.71	5.87 $\pm$ 0.50	66.5 $\pm$ 9.3	0.09 $\pm$ 0.04	24.5 $\pm$ 8.1	33 $\pm$ 10
<b>FSM-15</b>	80.4	0.60 $\pm$ 0.08	0.10	1.91 $\pm$ 0.65	0.35 $\pm$ 0.38	3.92 $\pm$ 0.16	46.4 $\pm$ 3.0	0.11 $\pm$ 0.02	15.9 $\pm$ 1.3	51.7 $\pm$ 3.6
<b>FSM-7</b>	76.8	0.35 $\pm$ 0.16	0.10	0.49 $\pm$ 0.35	0.38 $\pm$ 0.35	4.00 $\pm$ 0.35	18.04 $\pm$ 1.05	0.36 $\pm$ 0.09	17.75 $\pm$ 0.82	81.5 $\pm$ 1.4
<b>FSM-5</b>	74.8	0.23 $\pm$ 0.11	0.10	0.33 $\pm$ 0.21	0.56 $\pm$ 0.59	4.66 $\pm$ 0.28	37.99 $\pm$ 3.17	0.22 $\pm$ 0.05	20.83 $\pm$ 0.54	61.7 $\pm$ 3.4
<b>FSM-6</b>	74.4	0.75 $\pm$ 0.35	0.10	4.03 $\pm$ 4.46	0.31 $\pm$ 0.19	3.68 $\pm$ 1.4	18.6 $\pm$ 9.5	0.17 $\pm$ 0.13	16.05 $\pm$ 0.15	77.4 $\pm$ 5.1
<b>FSM-6LH</b>	74.4	0.86 $\pm$ 0.00	0.10	3.00 $\pm$ 0.10	0.09 $\pm$ 0.10	1.99 $\pm$ 0.06	6.6 $\pm$ 0.5	0.17 $\pm$ 0.01	15.71 $\pm$ 0.05	90.4 $\pm$ 0.6
<b>FSM-11</b>	65.2	0.66 $\pm$ 0.04	0.10	2.90 $\pm$ 0.88	0.27 $\pm$ 0.28	4.3 $\pm$ 2.0	49.5 $\pm$ 8.2	0.16 $\pm$ 0.04	7.18 $\pm$ 0.92	47.6 $\pm$ 7.3
<b>AI-I*</b>	1.0	1.05 $\pm$ 0.01	0.10	29.16 $\pm$ 1.45	0.08 $\pm$ 0.09	1.55 $\pm$ 0.12	38.5 $\pm$ 5.5	0.01 $\pm$ 0.00	11.8 $\pm$ 3.3	32.4 $\pm$ 7.0
<b>CLBR*</b>	0.5	1.03 $\pm$ 0.00	0.10	19.97 $\pm$ 0.08	0.09 $\pm$ 0.09	1.62 $\pm$ 0.01	26.70 $\pm$ 2.10	0.02 $\pm$ 0.00	13.75 $\pm$ 0.62	53.3 $\pm$ 2.2

6

7 Table S2. IRPL<sub>955</sub> lifetimes obtained for all samples investigated by fitting the off-time decay of the IRPL<sub>955</sub> with the sum of three exponential functions. The values in the table are  
 8 the average and standard deviation of two aliquots, which were measured per sample. *I* represents the intensity of each component,  $\tau$  the lifetime and *A* the amplitude (integrated  
 9 area under the curve). The different components are denoted using an index number. Prior to fitting the signals were normalised to the last data point of the on-time.

Sample ID	KFS [%]	<i>I</i> <sub>1</sub>	$\tau_1$ [ $\mu$ s]	<i>A</i> <sub>1</sub> [%]	<i>I</i> <sub>2</sub>	$\tau_2$ [ $\mu$ s]	<i>A</i> <sub>2</sub> [%]	<i>I</i> <sub>3</sub>	$\tau_3$ [ $\mu$ s]	<i>A</i> <sub>3</sub> [%]
<b>FSM-13</b>	98.5	0.09 ± 0.01	0.39 ± 0.01	0.24 ± 0.05	0.23 ± 0.25	5.89 ± 0.04	10.1 ± 1.9	0.64 ± 0.05	20.79 ± 0.50	89.7 ± 1.9
<b>FSM-13LH</b>	98.5	0.13 ± 0.00	0.53 ± 0.09	0.44 ± 0.07	0.17 ± 0.19	6.69 ± 0.98	8.1 ± 2.0	0.64 ± 0.03	21.96 ± 0.68	91.4 ± 2.1
<b>FSM-3</b>	82.5	0.05 ± 0.04	0.37 ± 0.04	0.28 ± 0.22	0.68 ± 0.74	4.48 ± 0.01	52.7 ± 5.6	0.19 ± 0.02	15.89 ± 0.08	47.0 ± 5.3
<b>FSM-15</b>	80.4	0.43 ± 0.01	0.14 ± 0.01	1.49 ± 0.03	0.51 ± 0.49	3.75 ± 0.05	47.2 ± 3.4	0.13 ± 0.01	15.94 ± 0.18	51.3 ± 3.4
<b>FSM-7</b>	76.8	0.09 ± 0.00	1.19 ± 0.01	1.24 ± 0.04	0.55 ± 0.53	4.30 ± 0.02	26.5 ± 2.3	0.35 ± 0.02	18.01 ± 0.02	72.2 ± 2.3
<b>FSM-5</b>	74.8	0.16 ± 0.06	1.4 ± 1.6	4.08 ± 4.9	0.69 ± 0.65	4.11 ± 0.64	43.9 ± 2.5	0.17 ± 0.01	19.2 ± 2.3	52.1 ± 2.4
<b>FSM-6</b>	74.4	0.87 ± 0.33	0.12 ± 0.00	7.5 ± 8.0	0.30 ± 0.18	6.54 ± 3.42	37.8 ± 9.8	0.10 ± 0.11	18.5 ± 3.7	55 ± 18
<b>FSM-6LH</b>	74.4	0.24 ± 0.06	0.27 ± 0.08	0.67 ± 0.03	0.23 ± 0.24	3.78 ± 0.33	9.7 ± 1.0	0.50 ± 0.00	16.71 ± 0.45	89.6 ± 1.1
<b>FSM-11</b>	65.2	0.25 ± 0.01	0.23 ± 0.07	1.72 ± 0.48	0.57 ± 0.55	3.02 ± 0.09	49.5 ± 6.1	0.20 ± 0.03	8.14 ± 0.17	48.8 ± 6.6
<b>AI-I</b>	1.0	0.89 ± 0.04	0.14 ± 0.01	18.9 ± 0.5	0.14 ± 0.17	2.09 ± 0.14	53 ± 13	0.02 ± 0.01	12.41 ± 0.11	28.4 ± 13.9
<b>CLBR</b>	0.5	0.49 ± 0.01	0.17 ± 0.02	1.62 ± 0.47	0.20 ± 0.19	2.19 ± 0.01	8.2 ± 1.8	0.28 ± 0.06	16.55 ± 0.68	90.1 ± 2.2

10

11

12